

RESEARCH ARTICLE

Multi-functional foot use during running in the zebra-tailed lizard (*Callisaurus draconoides*)

Chen Li¹, S. Tonia Hsieh² and Daniel I. Goldman^{1,*}

¹School of Physics, Georgia Institute of Technology, Atlanta, GA 30332, USA and ²Department of Biology, Temple University, Philadelphia, PA 19122, USA

*Author for correspondence (daniel.goldman@physics.gatech.edu)

SUMMARY

A diversity of animals that run on solid, level, flat, non-slip surfaces appear to bounce on their legs; elastic elements in the limbs can store and return energy during each step. The mechanics and energetics of running in natural terrain, particularly on surfaces that can yield and flow under stress, is less understood. The zebra-tailed lizard (*Callisaurus draconoides*), a small desert generalist with a large, elongate, tendinous hind foot, runs rapidly across a variety of natural substrates. We use high-speed video to obtain detailed three-dimensional running kinematics on solid and granular surfaces to reveal how leg, foot and substrate mechanics contribute to its high locomotor performance. Running at ~ 10 body lengths s^{-1} (~ 1 ms^{-1}), the center of mass oscillates like a spring-mass system on both substrates, with only 15% reduction in stride length on the granular surface. On the solid surface, a strut-spring model of the hind limb reveals that the hind foot saves $\sim 40\%$ of the mechanical work needed per step, significant for the lizard's small size. On the granular surface, a penetration force model and hypothesized subsurface foot rotation indicates that the hind foot paddles through fluidized granular medium, and that the energy lost per step during irreversible deformation of the substrate does not differ from the reduction in the mechanical energy of the center of mass. The upper hind leg muscles must perform three times as much mechanical work on the granular surface as on the solid surface to compensate for the greater energy lost within the foot and to the substrate.

Supplementary material available online at <http://jeb.biologists.org/cgi/content/full/215/18/3293/DC1>

Key words: terrestrial locomotion, mechanics, energetics, kinematics, spring-mass system, elastic energy savings, dissipation, granular media.

Received 23 June 2011; Accepted 31 May 2012

INTRODUCTION

Rapid locomotion such as running and hopping can be modeled as a spring-mass system bouncing in the sagittal plane [i.e. the spring-loaded inverted pendulum (SLIP) model] (Blickhan, 1989). This has been demonstrated in a variety of animals (Blickhan and Full, 1993; Holmes et al., 2006) in the laboratory on rigid, level, flat, non-slip surfaces (hereafter referred to as 'solid surfaces') such as running tracks and treadmills (Dickinson et al., 2000). In the SLIP model, the animal body [represented by the center of mass (CoM)] bounces on a single leg (represented by a spring) like a pogo stick, and exerts point contact on the solid ground. The leg spring compresses during the first half of stance, and then recoils during the second half of stance. Through this process, the mechanical (i.e. kinetic plus gravitational potential) energy of the CoM is exchanged with elastic energy stored in the compressed leg spring, reducing energy use during each step. For animals such as insects (e.g. Schmitt et al., 2002) and reptiles (e.g. Chen et al., 2006) that run with a sprawled limb posture, the CoM also oscillates substantially in the horizontal plane in a similar fashion, which can also be modeled as a spring-mass system bouncing in the horizontal plane [i.e. the lateral leg spring (LLS) model] (Schmitt et al., 2002). Both the SLIP and LLS models predict that the mechanical energy of the CoM is lowest at mid-stance and highest during aerial phase.

In these models, the spring-mass system and the interaction with the solid ground are perfectly elastic and do not dissipate energy, thus no net work is performed. However, as animals move across

natural surfaces, energy is dissipated both within their body and limbs (Fung, 1993) and to the environment (Dickinson et al., 2000). Therefore, mechanisms to reduce energy loss during locomotion can be important. The limbs of many organisms possess elastic elements such as tendons and ligaments that can function as springs to store and return energy during rapid locomotion such as running and hopping to decrease energetic cost (Alexander, 2003). Most notable for this function are the ankle extensor tendons in the lower hind leg and the digital flexor tendons and ligaments in the lower fore leg (Alexander, 2003). Furthermore, different limb-ground interaction strategies may be utilized depending on the dissipative properties of the substrate.

Laboratory experiments have begun to reveal mechanisms of organisms running on non-solid substrates, such as elastic (Ferris et al., 1998; Spence et al., 2010), damped (Moritz and Farley, 2003), inclined (Roberts et al., 1997) or uneven (Daley and Biewener, 2006; Sponberg and Full, 2008) surfaces, surfaces with few footholds (Spagna et al., 2007) and the surface of water (Glasheen and McMahon, 1996a; Hsieh, 2003). Although spring-mass-like CoM motion was observed only in some of these studies (Ferris et al., 1998; Moritz and Farley, 2003; Spence et al., 2010), a common finding is that on non-solid surfaces, limbs do not necessarily behave like springs to save energy. In addition, these studies suggest that both the active control of body and limb movement through the nervous system and the passive mechanical responses of viscoelastic limbs and feet with the environment play important roles in the

control of rapid terrestrial locomotion (for reviews, see Full and Koditschek, 1999; Dickinson et al., 2000).

Many substrates found in nature, such as sand, gravel, rubble, dirt, soil, mud and debris, can yield and flow under stress during locomotion. These substrates thus experience solid–fluid transitions, through which energy may be dissipated *via* plastic deformation. Understanding locomotion on such substrates is challenging in part because, unlike for flying and swimming, where the fluid flows and forces can in principle be determined by solving the Navier–Stokes equations in the presence of moving boundary conditions (Vogel, 1996), no comprehensive force models yet exist for terrestrial substrates that yield and flow (hereafter referred to as ‘flowing substrates’).

Granular materials (Nedderman, 1992), such as desert sand, which are composed of similarly sized particles, provide a good model substrate for studying locomotion on flowing substrates. Compared with other flowing substrates, granular materials are relatively simple and the intrusion forces within them can be modeled empirically (Hill et al., 2005). Their mechanical properties can also be precisely and repeatedly controlled using a fluidized bed (Li et al., 2009). In addition, locomotion on granular surfaces is directly relevant for many desert-dwelling reptiles and arthropods such as lizards, snakes and insects (Mosauer, 1932; Crawford, 1981). Recent advances in the understanding of force and flow laws in granular materials subject to localized intrusion (Hill et al., 2005; Katsuragi and Durian, 2007; Gravish et al., 2010; Ding et al., 2011) have begun to provide insight into the mechanics of locomotion on (and within) granular substrates (Li et al., 2009; Maladen et al., 2009; Mazouchova et al., 2010; Li et al., 2010b; Maladen et al., 2011).

The zebra-tailed lizard [*Callisaurus draconoides* Blainville 1835; snout–vent length (SVL) \sim 10 cm, mass \sim 10 g; Fig. 1A] is an excellent model organism for studying running on natural surfaces because of its high locomotor performance over diverse terrain. As a desert generalist, this lizard lives in a range of desert habitats including flat land, washes and sand dunes (Vitt and Ohmart, 1977; Korff and McHenry, 2011), and encounters a large variety of substrates ranging from rocks to gravel, closely packed coarse sand and loosely packed fine sand (Karasov and Anderson, 1998; Korff and McHenry, 2011). The zebra-tailed lizard is the fastest-running species among desert lizards of similar size (Irschick and Jayne, 1999a), and has been observed to run at up to 4 m s^{-1} [$50 \text{ body lengths s}^{-1}$] both on solid (e.g. treadmill) (Irschick and Jayne, 1999a) and on granular (e.g. sand dunes) (Irschick and Jayne, 1999b) surfaces. Its maximal acceleration and running speed also have been shown to not differ significantly when substrate changes from coarse wash sand to fine dune sand, whose yield strengths differ by a factor of three (Korff and McHenry, 2011).

Of particular interest is whether and how the zebra-tailed lizard’s large, elongate hind foot contributes to its high locomotor capacity. In addition to a slim body, a long tapering tail and slender legs (Fig. 1A), the zebra-tailed lizard has an extremely large, elongate hind foot, the largest (40% SVL) among lizards of similar size (Irschick and Jayne, 1999a). Its hind foot is substantially larger than the fore foot (area = 1 cm^2 versus 0.3 cm^2) and likely plays a dominant role in locomotion (Mosauer, 1932). Recent studies in insects, spiders and geckos (Jindrich and Full, 1999; Autumn et al., 2000; Dudek and Full, 2006; Spagna et al., 2007) have suggested that animals can rely on appropriate morphology and material properties of their bodies and limbs to accommodate variable, uncertain conditions during locomotion. Despite suggestions that the large foot area (Mosauer, 1932) and increased stride length *via* elongate toes may confer locomotor advantages (Irschick and Jayne, 1999a), the mechanisms of how the hind foot contributes to the zebra-tailed lizard’s high running ability remain unknown.

In this paper, we study the mechanics and mechanical energetics of the zebra-tailed lizard running on two well-defined model surfaces: a solid surface and a granular surface. These two surfaces lie on opposite ends of the spectrum of substrates that the zebra-tailed lizard encounters in its natural environment, and present distinct conditions for locomotion. We investigate whether the lizard’s center of mass (CoM) bounces like a spring-mass system during running on both solid and granular surfaces. We combine measurements of three-dimensional kinematics of the lizard’s body, hind limb and hind foot, dissection and resilience measurements of the hind limb, and modeling of foot–ground interactions on both substrates, and demonstrate that the lizard’s large, elongate hind foot serves different functions during running on solid and granular surfaces. We find that on the solid surface, the hind foot functions as an energy-saving spring; on the granular surface, it functions as a dissipative, force-generating paddle to generate sufficient lift during each step. The larger energy dissipation to the substrate and within the foot during running on the granular surface must be compensated for by greater mechanical work done by the upper hind leg muscles.

MATERIALS AND METHODS

Animals

Seven adult zebra-tailed lizards were collected from the Mojave Desert, AZ, USA, in August 2007 (Arizona Game and Fish Department, permit SP591773) for three-dimensional kinematics experiments. Table 1 shows the morphological measurements for

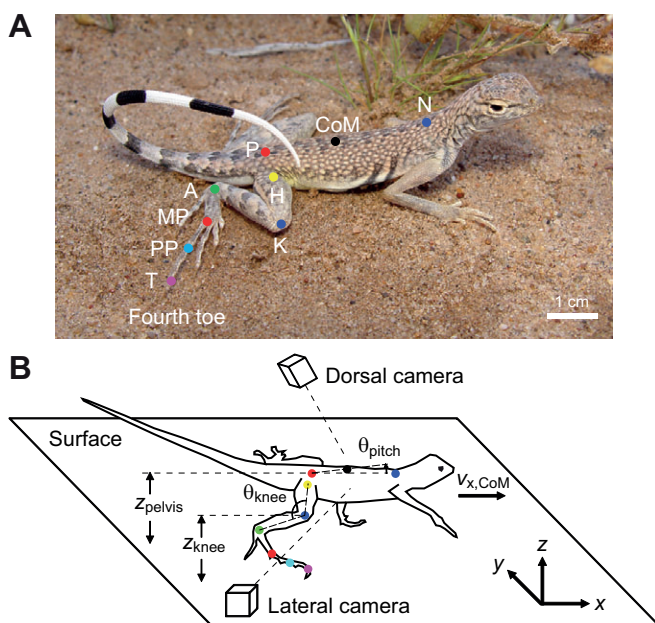


Fig. 1. Model organism and three-dimensional kinematics experiments. (A) A zebra-tailed lizard resting on sand in the wild (photo credit: Thomas C. Brennan). (B) Experimental setup for three-dimensional kinematics capture, with definitions of pelvis height (z_{pelvis}), knee height (z_{knee}), trunk pitch angle (θ_{pitch}) and knee angle (θ_{knee}). Colored dots in A and B are digitized points on the midline of the trunk, hind leg and elongate hind foot: neck (N), center of mass (CoM), pelvis (P), hip (H), knee (K), ankle (A), metatarsal-phalangeal joint (MP), distal end of the proximal phalanx (PP) and digit tip (T) of the fourth toe. $v_{x,\text{CoM}}$, forward speed.

Table 1. Morphological measurements of the seven *Callisaurus draconoides* tested in the three-dimensional kinematics experiments

Parameter	Mean \pm s.d.
Snout–vent length (cm)	7.2 \pm 0.6
Mass (g)	11.0 \pm 2.7
Trunk length (cm)	4.4 \pm 0.4
Pelvic width (cm)	1.4 \pm 0.1
Hind limb length (cm)	6.4 \pm 0.1
Hind foot length (cm)	2.7 \pm 0.1
Femur length (cm)	1.6 \pm 0.2
Tibia length (cm)	2.1 \pm 0.2
Tarsal and metatarsal length (cm)	1.0 \pm 0.1
Fourth toe length (cm)	1.7 \pm 0.1

these seven animals. Eleven additional adult animals were collected from the Mojave Desert, CA, USA, in September 2009 (California Department of Fish and Game, permit SC 10901) for hind limb resilience measurements. Two preserved specimens were used for dissection. The animals were housed in the Physiological Research Laboratory animal facility of The Georgia Institute of Technology. Each animal was housed individually in an aquarium with a sand substrate, and was fed crickets and mealworms dusted with a vitamin and calcium supplement two to three times per week. The ambient temperature was maintained at 28°C during the day and 24°C during the night. Full-spectrum fluorescent bulbs high in ultraviolet B were set to a 12 h:12 h light:dark schedule. Ceramic heating elements were provided 24 h per day to allow the animals to thermoregulate at preferred body temperature. All experimental procedures were conducted in accordance with The Georgia Institute of Technology IACUC protocols.

Surface treatments

A wooden board (120 \times 23 \times 1 cm³) bonded with sandpaper (grit size \sim 0.1 mm) for enhanced traction was used as the solid surface. Glass particles (mean \pm s.d. diameter=0.27 \pm 0.04 mm, density=2.5 \times 10³ kg m⁻³, Jaygo, Union, NJ, USA) were used as the granular substrate; the particles are approximately spherical and of similar size to typical desert sand (Dickinson and Ward, 1994). Before each trial, a custom-made fluidized bed trackway (200 \times 50 cm, length \times width) prepared the granular substrate (12 cm deep) into a loosely packed state (volume fraction=0.58) for repeatable yield strength [for experimental details of the fluidized bed trackway, see Li et al. (Li et al., 2009)].

Three-dimensional kinematics

We used high-speed video to obtain three-dimensional kinematics as the lizard ran across the prepared surfaces (Fig. 1B). Before each session, high-contrast markers (Wite-Out, Garden Grove, CA, USA) were painted on each animal for digitizing at nine joints along the midline of the trunk and the right hind limb (Fig. 1): neck (N), CoM, pelvis (P), hip (H), knee (K), ankle (A), metatarsal-phalangeal joint (MP), distal end of the proximal phalanx (PP) and digit tip (T) of the fourth toe. The approximate longitudinal location of the CoM in resting position was determined by tying a thread around the body of an anesthetized lizard and repositioning the thread until the body balanced horizontally. Before each trial, the surface was prepared (for the granular surface treatment only), and calibration images were taken of a custom-made 39-point calibration object (composed of LEGO, Billund, Denmark). The animal was then induced to run across the field of view by a slight tap or pinch on the tail. Two

synchronized high-speed cameras (AOS Technologies, Baden Daettwil, Switzerland) captured simultaneous dorsal and lateral views at 500 frames s⁻¹ (shutter time=300 μ s). The ambient temperature was maintained at 35°C during the test. Animals were allowed to rest for at least 5 min between trials and for at least 2 days between sessions.

We digitized the calibration images and high-speed videos, and used direct linear transformation (DLT) to reconstruct three-dimensional kinematics from the two-dimensional kinematics from both dorsal and lateral views. Digitization and DLT calculations were performed using custom software [DLTcal5 and DLTdv5 (Hedrick, 2008)]. Axes were set such that +x pointed in the direction of forward motion, +z pointed vertically upward and +y pointed to the left of the animal. Footfall patterns of touchdown and takeoff were determined from the videos. On the granular surface, because the hind foot often remained obscured by splashed particles during foot extraction, we defined foot takeoff as when the knee began to flex following extension during limb protraction (which is when foot takeoff occurs on the solid surface). To reduce noise and enable direct comparisons among different running trials, position data were filtered with a Butterworth low-pass filter with a cut-off frequency of 75 Hz, and interpolated to 0–100% of one full stride period (T) between two successive touchdowns of the right hind limb. All data analysis was completed with MATLAB (MathWorks, Natick, MA, USA) unless otherwise specified.

Statistics

We accepted trials that met the following criteria: the animal ran continuously through the field of view, the run was straight without contacting sidewalls of the trackway, there was a full stride (between two consecutive touchdowns of the right hind limb) in the range of view, all nine markers were visible throughout the full stride, and the forward speed changed by less than 20% after the full stride. With these criteria, out of a total of 125 trials from seven individuals on both solid (61 trials from seven individuals) and granular (64 trials from seven individuals) surfaces collected over a period of over three months, we ultimately accepted 51 runs from seven individuals on solid (23 runs) and granular (28 runs) surfaces. Because the data set had an unequal number of runs per individual, and because we were measuring freely running animals and did not control for speed, to maintain statistical power, all statistical tests were performed on a subset of these data using one representative run per individual on both solid ($N=7$) and granular ($N=7$) surfaces. The representative run for each individual was selected based on having the most consistent running speed for at least one full stride and was also closest to the mean running speed of all 51 trials. Data are reported as means \pm s.d. from the seven representative runs on each substrate unless otherwise specified.

To determine the effect of substrate, all kinematic variables were corrected for size-related differences by regressing the variables against SVL and taking the residuals for those that regressed significantly with SVL ($P<0.05$). We then ran an ANCOVA with substrate and speed as covariates to test for substrate effects, independent of running speeds. All statistical tests were performed using JMP (SAS Institute, Cary, NC, USA).

For the energetics data, we used dimensionless quantities by normalizing energies of each run to the CoM mechanical energy at touchdown of that run, thus eliminating the effect of mass and running speed on energies. An ANOVA was used to test for differences between the reduction in CoM mechanical energy, elastic energies and energy loss. A Tukey's honestly significant difference (HSD) test was used for *post hoc* testing where needed.

Dissection and model of the hind limb

To gain insight into the role of anatomical components of the hind limb on mechanics during locomotion, we dissected the hind limb of two preserved specimens. We quantified anatomical dimensions by measuring the radii of the knee (K), ankle (A), the metatarsal-phalangeal joint (MP), the distal end of the proximal phalanx (PP) and the digit tip (T) of the fourth toe. We also observed the muscle and tendon arrangements within the lower leg and the foot. Based on these anatomical features, we developed a model of the hind limb that incorporated the structure, properties and function of its main elements.

Resilience measurements of the hind limb

To characterize the resilience of the hind limb for estimation of energy return, a modification of the work loop technique was used (Fig. 2A), in which the limb was kept intact and forces were applied to the whole limb instead of a single muscle (Dudek and Full, 2006). The animal was anesthetized using a 2% isoflurane air solution during the test. The hind foot was maintained within the vertical plane, pushed down onto and then extracted from a custom force platform that was suited to small animals ($10.2 \times 7.6 \text{ cm}^2$, range=2.5 N, resolution=0.005 N) and bonded with sandpaper (grit size $\sim 0.1 \text{ mm}$). Ground reaction force F was measured at a sampling rate of 10 kHz using a custom LabVIEW program (National

Instruments, Austin, TX, USA). At the same time, a Phantom high-speed camera (Vision Research, Wayne, NJ, USA) recorded deformation of the foot from the side view at $250 \text{ frames s}^{-1}$ (shutter time=500 μs). High-contrast markers (Wite-Out) were painted on the joints of the hind foot (A, MP, PP, T and a point on the tibia above the ankle). The ambient temperature was maintained at 35°C during the test.

Videos of foot deformation were digitized to obtain the angular displacement of the foot $\Delta\theta = \theta_0 - \theta_t$, i.e. the change in the angle formed by the tibia and the foot (from the ankle to the digit tip of the fourth toe) (Fig. 2A). Angular displacement was synchronized with the measured torque τ about the ankle (calculated from the measured ground reaction force) to obtain a passive work loop. The damping ratio of the hind limb, i.e. the percentage of energy lost within the hind limb after loading and unloading, was calculated as the fraction of area within a work loop relative to the area under the higher loading curve (Fung, 1993). Hind limb resilience, i.e. the percentage of energy returned by the foot after loading and unloading, was one minus the damping ratio (Ker et al., 1987; Dudek and Full, 2006). An ANOVA was used to test the effect of maximal torque, maximal angular displacement, loading rate and individual animal on hind limb resilience.

Granular penetration force measurements

Although comprehensive force models are still lacking to calculate ground reaction forces during locomotion granular media, a low-speed penetration force model was previously used to explain the locomotor performance of a legged robot on granular media (Li et al., 2009). Similarly, to estimate the vertical ground reaction force on the lizard foot during running on the granular surface, we measured the vertical force on a plate slowly penetrating vertically into the granular substrate (Fig. 2B). Before each trial, a fluidized bed (area= $24 \times 22 \text{ cm}^2$) prepared the granular substrate (depth=12 cm) into a loosely packed state (volume fraction=0.58) (for details, see Maladen et al., 2009). A robotic arm (CRS Robotics, Burlington, ON, Canada) pushed a horizontally oriented plate vertically downward at 0.01 m s^{-1} into the granular substrate to a depth of 7.6 cm, and then extracted the plate vertically at 0.01 m s^{-1} . The force on the plate was measured by a force transducer (ATI Industrial Automation, Apex, NC, USA) mounted between the robotic arm and the plate at a sampling rate of 100 Hz using a custom LabVIEW program. The depth of the plate was measured by tracking the position of an LED light marker mounted on the robotic arm in side view videos taken by a Pike high-speed camera (Edmund Optics, Barrington, NJ, USA). Two thin aluminum plates of different area were used ($A_1 = 7.6 \times 2.5 \text{ cm}^2$ and $A_2 = 3.8 \times 2.5 \text{ cm}^2$; thickness=0.6 cm). Three trials were performed for each plate.

RESULTS

Performance and gait

On both solid and granular surfaces, the zebra-tailed lizard ran with a diagonal gait, a sprawled limb posture and lateral trunk bending (see Fig. 3 and supplementary material Movies 1, 2 for representative runs on both substrates). Fig. 4 shows mean forward speed $\bar{v}_{x, \text{CoM}}$, stride frequency f and duty factor D of the entire data set (all symbols; 23 runs on the solid surface and 28 runs on the granular surface) and of the representative runs (filled symbols; $N=7$ on the solid surface and $N=7$ on the granular surface). Table 2 lists mean values and statistical results for all the gait and kinematic variables from the representative runs for both solid ($N=7$) and granular ($N=7$) surfaces. On both surfaces, $\bar{v}_{x, \text{CoM}}$ increased with f (ANCOVA, $P < 0.05$; Fig. 4A), and D decreased with $\bar{v}_{x, \text{CoM}}$ (ANCOVA, $P < 0.05$;

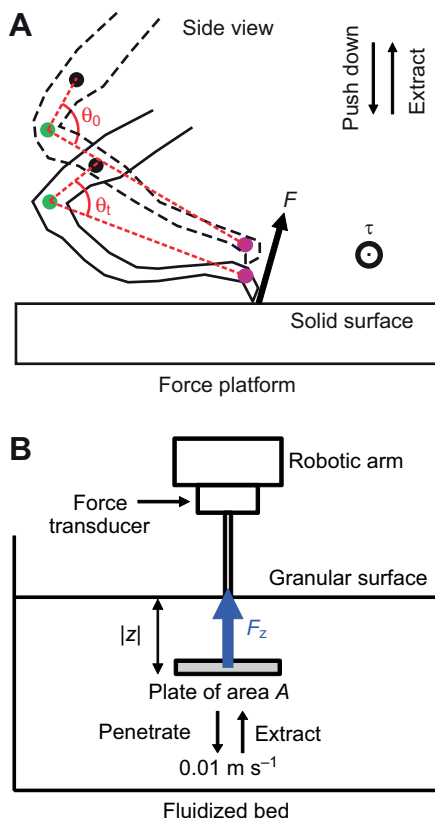


Fig. 2. Setup of experiments to measure hind limb resilience and granular penetration force. (A) Experimental setup for hind limb resilience measurements. Dashed tracing shows the relaxed, straight foot right before touchdown. Solid tracing shows the hyperextended foot during ground contact. F , ground reaction force; θ_0 , angle between the ankle and the digit tip in the relaxed, straight foot; θ_t , angle between the ankle and the digit tip in the hyperextended foot; τ , torque about the ankle. (B) Experimental setup for granular penetration force measurements. F_z , vertical ground reaction force; $|z|$, depth.

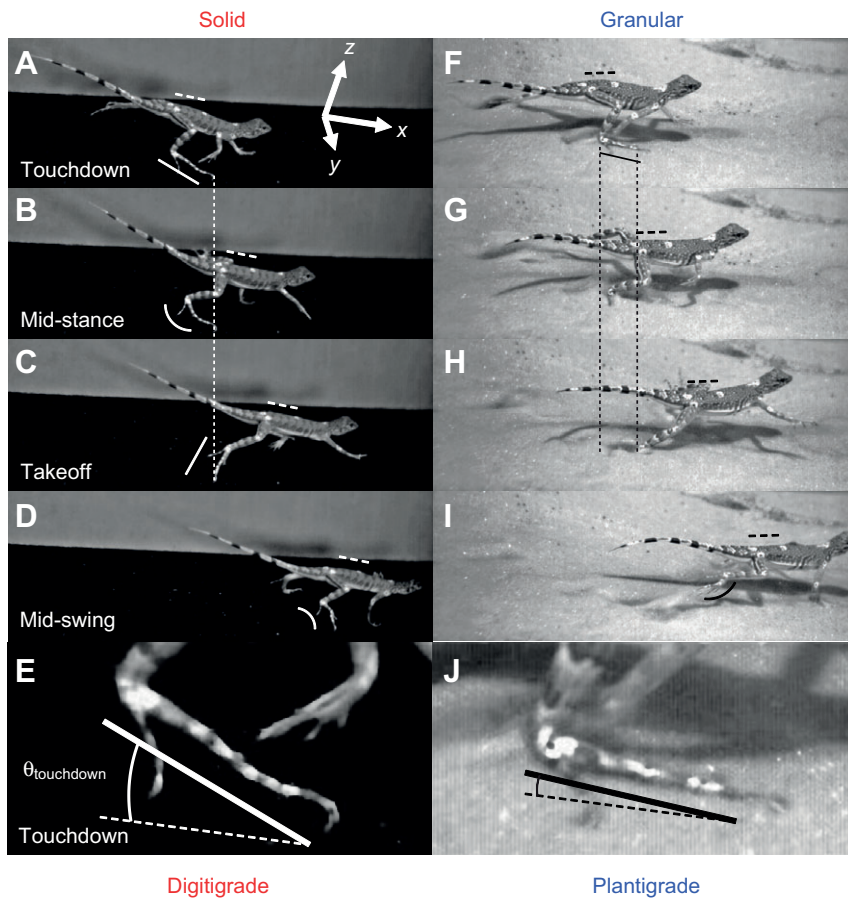


Fig. 3. Lateral views of representative runs on the solid (A–D) and granular (F–I) surfaces (see supplementary material Movies 1, 2). (E, J) Closer views of foot posture at touchdown showing definition of touchdown foot angle, $\theta_{\text{touchdown}}$. Solid lines and curves along the foot indicate hind foot posture and shape. Note that the lateral camera was oriented at an angle to the x -, y - and z -axes such that forward (+ x) direction appeared to point slightly downwards.

Fig. 4B). D was ~ 0.45 on both surfaces, resulting in an aerial phase of $\sim 5\%$ of stride period T between alternating stances (Fig. 5A). Neither $\bar{v}_{x, \text{CoM}}$ (ANOVA, $P > 0.05$) nor D (ANCOVA, $P > 0.05$) significantly differed between surfaces. Stride length, $\lambda = \bar{v}_{x, \text{CoM}}/f$, was 15% shorter on the granular surface (ANCOVA, $P < 0.05$).

CoM kinematics

The lizards displayed qualitatively similar CoM oscillations during running on both surfaces. The CoM forward speed $\bar{v}_{x, \text{CoM}}$ (Fig. 5B) and vertical position z_{CoM} (Fig. 5C) oscillated at $2f$, dropping during the first half and rising during the second half of a stance, i.e. reaching a minimum at mid-stance and a maximum during the aerial phase. The CoM also oscillated medio-laterally at f (Fig. 5D). Throughout the entire stride, z_{CoM} was significantly higher on the solid surface (ANCOVA, $P < 0.05$). The CoM vertical oscillations Δz_{CoM} and lateral oscillations Δy_{CoM} did not differ between substrates (ANCOVA, $P > 0.05$).

Hind foot, hind leg and trunk kinematics

The lizards displayed distinctly different hind foot, hind leg and trunk kinematics during running on solid and granular surfaces (Figs 3, 6). On the solid surface, the lizards used a digitigrade foot posture (Fig. 3A–E, solid line/curve). During the entire stride, the hind foot engaged the solid surface only with the digit tips. At touchdown, the toes were straight and pointed slightly downward. The touchdown foot angle $\theta_{\text{touchdown}}$ (measured along the fourth toe) was 12 ± 4 deg relative to the surface (Fig. 3A, E, Fig. 6A, red). During stance, the long toes pivoted over the stationary digit tips (Fig. 3A–C; vertical dotted line shows zero displacement) and hyperextended into a C-shape (Fig. 3B, solid curve). The foot

straightened again at takeoff, pointing downward and slightly backward (Fig. 3C, solid line), and then flexed during swing (Fig. 3D, solid curve).

On the granular surface, the lizards used a plantigrade foot posture (Fig. 3F, I, solid line). At touchdown, the hind foot was nearly parallel with the surface, with the toes spread out and held straight. In the vertical direction, the foot impacted the granular surface at speeds of up to 1 ms^{-1} . The ankle joint slowed to $\sim 0.1 \text{ ms}^{-1}$ within a few milliseconds following impact (a small percentage of stride period T) while the foot started penetrating the surface. The touchdown foot angle $\theta_{\text{touchdown}}$ was 4 ± 3 deg relative to the surface (Fig. 3J, Fig. 6A, blue), significantly smaller than that on the solid surface (ANCOVA, $P < 0.05$). During stance, the entire foot moved subsurface and was obscured (Fig. 3G). The ankle joint remained visible right above the surface and moved forward by approximately one foot length (Fig. 3F–H, vertical dotted line shows ankle displacement). The foot was extracted from the substrate at takeoff, pointing downward and slightly backward, and then flexed during swing (Fig. 3I, solid curve).

As a result of foot penetration on the granular surface, both the knee height z_{knee} (Fig. 6B) and the pelvis height z_{pelvis} (Fig. 6C) were lower on the granular surface (ANCOVA, $P < 0.05$). In addition, on the granular surface, the knee moved downward by a larger vertical displacement Δz_{knee} during the first half of stance (ANCOVA, $P < 0.05$; Fig. 6B), while the knee joint extended by a larger angle $\Delta \theta_{\text{knee}}$ during the second half of stance (ANCOVA, $P < 0.05$; Fig. 6D). Throughout the entire stride, the trunk was nearly horizontal on the solid surface (Fig. 3A–D, dashed line), but pitched head-up on the granular surface (Fig. 3F–I, dashed line; Fig. 6E). On both surfaces, the hind legs were sprawled at an angle (θ_{sprawl}) of ~ 40 deg during stance (θ_{sprawl} is defined as the angle between the horizontal

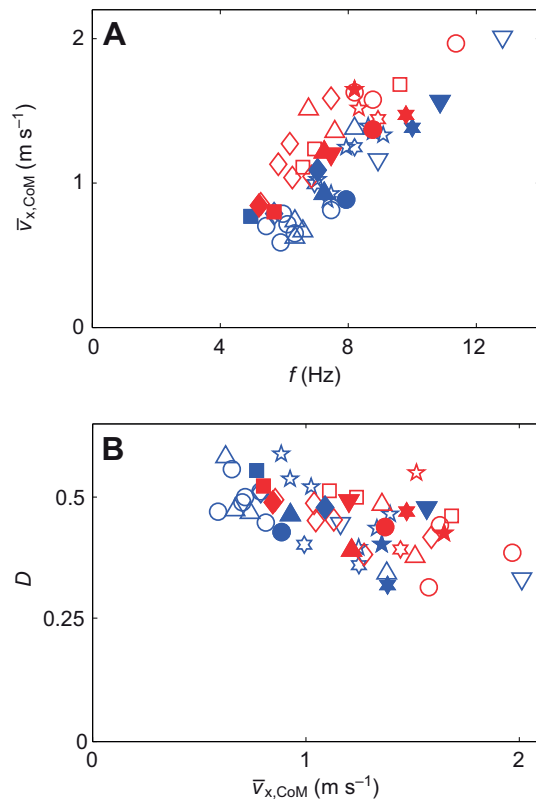


Fig. 4. Performance and gait on the solid (red) and granular (blue) surfaces. (A) Mean forward speed ($\bar{v}_{x,CoM}$) versus stride frequency (f). (B) Duty factor (D) versus mean forward speed. Different symbols represent different individuals. Filled symbols are from the seven representative runs for each of the seven individuals tested on both substrates. Open symbols are from runs that were not included in the representative data set.

plane and the leg orientation in the posterior view; Fig. 3). In most runs, the tail was farther from the solid surface and closer to the granular surface (Fig. 3).

Hind limb anatomy

From morphological measurements (Table 1), the hind foot of the zebra-tailed lizard comprised 42% of the hind limb length, and the longest fourth toe alone accounted for 63% of the hind foot length. These ratios are in a range similar to previous observations (Irschick and Jayne, 1999a). The slender foot had a cross-sectional radius r of 0.50–1.25 mm tapering distally, with reducing joint radii: $r_K=r_A=1.25$ mm, $r_{MP}=0.75$ mm, $r_{PP}=r_T=0.50$ mm.

Unlike many cursorial mammals whose ankle extensor muscles of the lower hind leg have long tendons (Alexander, 2003), ankle extensor tendons are nearly non-existent in the zebra-tailed lizard (Fig. 7A). Instead, layers of elongate tendons are found in both the dorsal and ventral surfaces of the foot. Our anatomical description is focused on the ventral muscle and tendon anatomy in the hind limb and terms given to muscles and tendons follow Russell (Russell, 1993). A large, tendinous sheath, the superficial femoral aponeurosis, originates from the femoro-tibial gastrocnemius, stretches across the ventral surface of the foot, and inserts on the metatarsal-phalangeal joints for digits III and IV. The superficial portion of the femoro-tibial gastrocnemius muscle body extends to the base of the ankle, thereby rendering the human equivalent of the ankle extensor tendons (i.e. the ‘Achilles’ tendon) absent. Deep to the superficial femoral

aponeurosis lie the flexor digitorum brevis muscles (not shown), which control the flexion of each of the digits. Tendons from the flexor digitorum longus muscle located on the lower hind leg run deep to the flexor digitorum brevis muscle bodies, and extend to the tips of the digits. No additional tendons are visible deep to the flexor digitorum longus tendons.

Hind limb model

Based on the observed muscle and tendon anatomy, we propose a two-dimensional strut-spring model of the hind limb (Fig. 7B), which assumes isometric contraction for the lower leg muscles and incorporates the spring nature of the foot tendons. This model is inspired from previous observations in large running and hopping animals of the strut-like function of ankle extensor muscles (Biewener, 1998a; Roberts et al., 1997) and spring-like function of ankle extensor tendons (for a review, see Alexander, 2003). Rigid segments (Fig. 7B, dashed lines), which are free to rotate about joints within a plane, represent the skeleton. The ankle extensor muscles in the lower leg, which originate on the femur and run along the ventral side of the tibia, are modeled as a rigid strut (muscle strut, blue line, Fig. 7B) that contracts isometrically during stance in running. A linear spring (tendon spring, red line, Fig. 7B), which originates from the distal end of the muscle strut and extends to the digit tip, models the elastic foot tendons. The muscle strut and tendon spring are ventrally offset from the midline of the skeleton at each joint by respective joint radii.

Hind limb resilience

Representative passive work loops (Fig. 8A–C) showed that torque τ was higher when the foot was pushed down on the solid surface than when it was extracted, similar to previous observations in humans (Ker et al., 1987) and cockroaches (Dudek and Full, 2006). Maximal torque was positively correlated with maximal angular displacement (ANOVA, $F_{1,62}=64.3188$, $P<0.001$). The kinks observed in the middle of the loading curve were due to the fifth toe contacting the surface. Mean hind limb resilience R calculated from the work loops was 0.44 ± 0.12 (three individuals, 64 trials; Fig. 8D–F). R did not differ between individuals (ANOVA, $F_{2,61}=2.1025$, $P=0.1309$), and did not depend on maximal torque (ANOVA, $F_{1,62}=0.5208$, $P=0.4732$; Fig. 8D), maximal angular displacement (ANOVA, $F_{1,62}=0.0164$, $P=0.8987$; Fig. 8E) or loading rate ($F_{1,62}=1.1228$, $P=0.2934$, ANOVA; Fig. 8F).

Hind foot curvature, tendon deformation and tendon stiffness

The observed three-dimensional positions of the hind limb fit well to the two-dimensional hind limb model (Fig. 9A–D), and enabled calculation of the curvature, tendon deformation and tendon stiffness of the hind foot (see Appendix). Calculated hind foot curvature κ (Fig. 9E, solid curve) showed that the hind foot hyperextended during stance (positive κ) and flexed during swing (negative κ). The foot was straight at touchdown and shortly after takeoff ($\kappa=0$). Calculated tendon spring deformation Δl (Fig. 9E, dashed curve) showed that the tendon spring stretched during the first half and recoiled during the second half of stance. The estimated tendon spring stiffness was 4.4×10^3 N m⁻¹ (see Appendix).

Mechanical energetics on the solid surface

Using the observed CoM and hind limb kinematics, calculated tendon spring stiffness and deformation, and measured hind limb resilience, we examined the mechanical energetics of the lizard running on the solid surface (Table 3, Fig. 9F). From the observed CoM kinematics, in the first half of stance, the mechanical energy

Table 2. Gait and kinematic variables (means \pm s.d.) and results of an ANCOVA testing for the effect of surface

Variable	Solid	Granular	$F_{2,11}$	P
Mean forward speed $\bar{v}_{x,CoM}$ ($m s^{-1}$)*	1.2 \pm 0.3	1.1 \pm 0.3	0.4784	0.5023
Stride frequency, f (Hz)	7.5 \pm 1.6	8.1 \pm 2.0	9.9101	0.0319
Duty factor, D	0.46 \pm 0.05	0.45 \pm 0.07	0.5032	0.5480
Stride length, λ (m)	0.16 \pm 0.02	0.14 \pm 0.02	8.9112	0.0409
Mean CoM height, \bar{z}_{CoM} (cm)	3.2 \pm 0.7	2.2 \pm 0.5	5.4690	0.0203
Magnitude of CoM vertical oscillations, Δz_{CoM} (cm)	0.3 \pm 0.2	0.4 \pm 0.3	3.7031	0.4697
Lowest CoM height (cm)	3.0 \pm 0.7	2.0 \pm 0.4	7.7544	0.0115
Time of lowest CoM height (T)	0.18 \pm 0.04	0.19 \pm 0.04	0.9696	0.6366
Highest CoM height (cm)	3.3 \pm 0.7	2.4 \pm 0.6	3.6126	0.0447
Time of highest CoM height (T)	0.44 \pm 0.04	0.48 \pm 0.01	3.0642	0.0325
Magnitude of CoM lateral oscillations, Δy_{CoM} (cm)	0.86 \pm 0.19	0.94 \pm 0.23	0.2350	0.5263
Mean pelvis height, \bar{z}_{pelvis} (cm)	3.1 \pm 0.7	1.9 \pm 0.5	8.8912	0.0046
Mean trunk pitch angle, $\bar{\theta}_{pitch}$ (deg)	1 \pm 3	9 \pm 2	19.5282	0.0002
Touchdown knee height (cm)	2.7 \pm 0.7	1.7 \pm 0.6	6.7157	0.0171
Lowest knee height (cm)	1.8 \pm 0.5	0.7 \pm 0.4	15.4261	0.0006
Knee vertical displacement during the first half of stance, Δz_{knee} (cm)	0.9 \pm 0.2	1.1 \pm 0.4	0.7128	0.3056
Touchdown knee angle (deg)	88 \pm 25	90 \pm 13	1.2344	0.6713
Lowest knee angle (deg)	79 \pm 17	79 \pm 10	1.3175	0.7549
Highest knee angle (deg)	116 \pm 15	150 \pm 8	17.568	0.0001
Knee joint extension during stance, $\Delta\theta_{knee}$ (deg)	37 \pm 13	71 \pm 4	18.0994	0.0001
Mean leg sprawl angle during stance, $\bar{\theta}_{sprawl}$ (deg) [†]	40 \pm 1	38 \pm 5	n/a	n/a
Touchdown foot angle, $\theta_{touchdown}$ (deg)	12 \pm 4	4 \pm 3	7.6973	0.0032

All significant differences ($P < 0.05$) are in bold.

*An ANOVA was used to test the effect of surface on running speed.

[†]A direct comparison was not possible for $\bar{\theta}_{sprawl}$ between surfaces because it was measured differently: on the solid surface, leg orientation was measured from the hip to the digit tip; on the granular surface, leg orientation was measured from the hip to the ankle. CoM, center of mass.

of the CoM (kinetic energy plus gravitational potential energy) decreased significantly from $E_{touchdown}=1.00\pm 0.00$ at touchdown to $E_{mid-stance}=0.81\pm 0.08$ at mid-stance (ANOVA, $F_{2,18}=12.2345$, $P=0.0004$; Tukey's HSD). In the second half of stance, the mechanical energy of the CoM recovered to $E_{aerial}=0.95\pm 0.10$ at mid aerial phase, not significantly different from $E_{touchdown}$ (Tukey's HSD). The reduction in CoM mechanical energy in the first half of stance, $\Delta E_{mech}=0.19\pm 0.08$, is the mechanical work needed per step on the solid surface. Note that the energies of each run were normalized to $E_{touchdown}$ of that run.

At mid-stance, the elastic energy stored in the tendon spring was $E_{storage}=0.18\pm 0.13$ (calculated from $1/2k\Delta l_{max}^2$, see Appendix), and was not significantly different from ΔE_{mech} (ANOVA, $F_{1,12}=0.0475$, $P=0.8312$). Because hind limb resilience R is equal to 0.44 ± 0.12 , the elastic recoil of the foot tendons returned an energy of $E_{return}=RE_{storage}=0.08\pm 0.06$, or $41\pm 33\%$ of the mechanical work needed per step (ΔE_{mech}) on the solid surface. We verified that foot flexion during swing induced little energy storage ($<0.1E_{storage}$) because the hind foot was less stiff during flexion ($0.7\times 10^3 N m^{-1}$) than during hyperextension ($4.4\times 10^3 N m^{-1}$).

Granular penetration force model

Although little is known about the kinematics and mechanics of the complex limb intrusions during legged locomotion on granular surfaces, we took inspiration from previous observations that horizontal drag (Maladen et al., 2009) and vertical impact (Katsuragi and Durian, 2007) forces in glass particles were insensitive to speed when intrusion speed was below $\sim 0.5 m s^{-1}$. Because the kinematics observed on the granular surface suggest that the vertical speeds of most of the foot relative to the ground were below $0.5 m s^{-1}$ during most of the stance phase (see Appendix), we assumed that the ground reaction forces on the lizard's feet were also insensitive to speed. This allowed us to use the vertical penetration force measured at

$0.01 m s^{-1}$ to model and estimate the vertical ground reaction forces on the lizard foot.

From the force data on both plates (Fig. 10), vertical ground reaction force F_z was proportional to both penetration depth $|z|$ and projected area A of the plate (area projected into the horizontal plane). During penetration, F_z was pointing upward; during extraction, F_z was pointing downward and dropped by an order of magnitude. These measurements were in accord with previous observations of forces on a sphere penetrating into granular media (Hill et al., 2005). Furthermore, we estimated from free falling of particles under gravity that it would take longer than the stance duration (45 ms) for the particles surrounding a penetrating foot to refill a hole created by the foot of maximal depth ($|z|_{max}=1.0$ cm, see Appendix). Thus we assumed that the vertical ground reaction forces were negligible during foot extraction.

Therefore, we approximate the vertical penetration force as:

$$F_z = \begin{cases} \alpha|z|A, & \text{for increasing } |z|, \\ 0, & \text{for decreasing } |z|, \end{cases} \quad (1)$$

where α is the vertical stress per unit depth, which is determined by the properties of the granular material and increases with compaction (Li et al., 2009). Fitting $F_z=\alpha|z|A$ to the force data during penetration over regions where the plate was fully submerged and far from boundary (Fig. 10, dashed lines), we obtained $\alpha=3.5\times 10^5 N m^{-3}$ for loosely packed 0.27 ± 0.04 mm diameter glass particles.

Vertical ground reaction force on the granular surface

During a stance on the granular surface, the CoM vertical speed $v_{z,CoM}$ (calculated from z_{CoM}) was approximately sinusoidal (Fig. 11A, dashed curve). This implies that the F_z on a lizard foot must be approximately sinusoidal. In addition, the foot was nearly

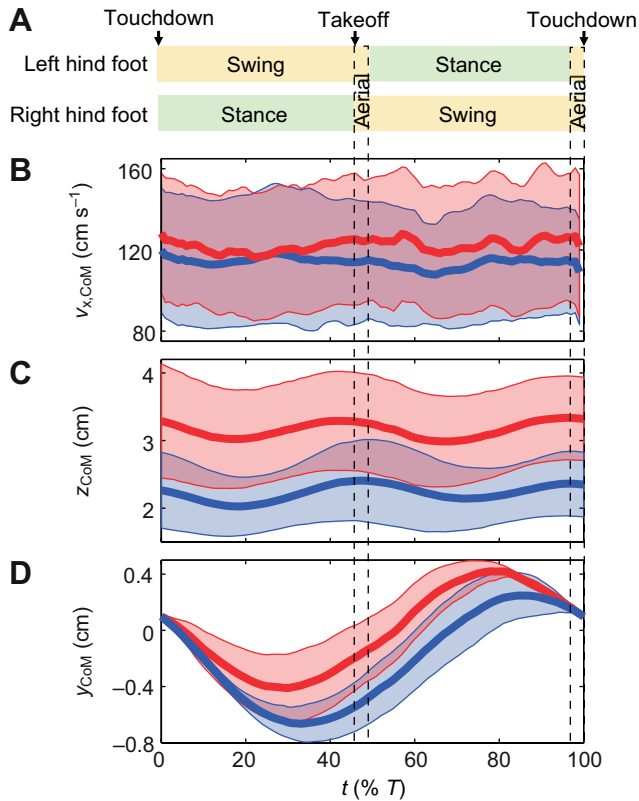


Fig. 5. Center of mass (CoM) kinematics (means \pm s.d.) versus time (t , % of stride period T) during a stride on the solid (red) and granular (blue) surfaces. (A) Footstep pattern; (B) CoM forward speed ($v_{x,CoM}$); (C) CoM vertical position (z_{CoM}); (D) CoM lateral position (y_{CoM}).

horizontal at touchdown, but pointed downward and slightly backward during takeoff. In consideration of the functional form of the penetration force (Eqn 1), we hypothesized that during stance the foot rotated subsurface by $\pi/2$ in the sagittal plane (Fig. 11C), increasing foot depth $|z|$ but decreasing projected foot area A , thus resulting in a sinusoidal F_z , which reaches a maximum at mid-stance before the foot reaches largest depth (see Appendix). A sinusoidal F_z is also possible for a fixed projected foot area if the foot maintains contact on solidified particles. However, this is unlikely considering that during stance the ankle moved forward at the surface level by a foot length.

Assuming that during stance the hind foot rotated by $\pi/2$ in the sagittal plane at a constant angular velocity, the vertical ground reaction force that each foot generated was $F_z = 5\pi mg/9 \sin 10\pi t/9T$, where t is time (see Appendix). The net vertical acceleration due to this F_z and the animal weight mg was $a_z = F_z/m - g$ (Fig. 11B; solid and dashed curves are a_z from both hind feet, shifted from each other by $T/2$). The CoM vertical speed $v_{z,CoM}$ predicted from the total a_z on both hind feet (Fig. 11A, dashed curve) agreed with experimental observations (Fig. 11A, solid curve). The slight underprediction of the oscillation magnitudes of $v_{z,CoM}$ was likely a result of an overestimation of duty factor on the granular surface. This is because F_z may have dropped to zero even before takeoff if the foot started moving upward before takeoff (Fig. 10).

Mechanical energetics on the granular surface

Using the measured CoM kinematics, assumed foot rotation and calculated vertical ground reaction force, we examined the

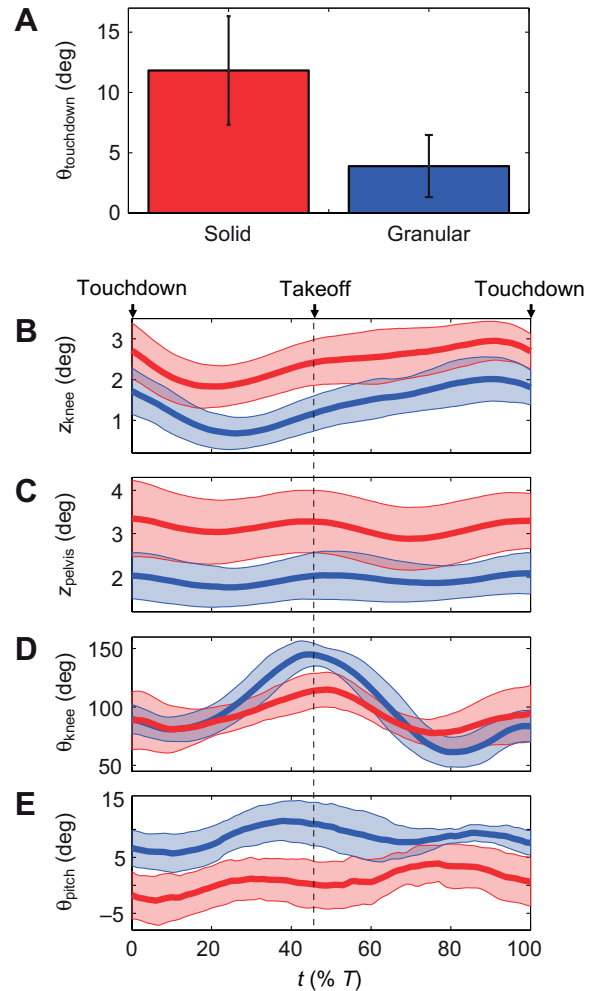


Fig. 6. Hind foot, hind leg and trunk kinematics (means \pm s.d.) versus time during a stride on the solid (red) and granular (blue) surfaces. (A) Touchdown foot angle ($\theta_{touchdown}$); (B) knee height (z_{knee}); (C) pelvis height (z_{pelvis}); (D) knee angle (θ_{knee}); (E) trunk pitch angle (θ_{pitch}). See Fig. 1 and Fig. 3E,J for illustrations of kinematic variables.

mechanical energetics of the lizard running on the granular surface (Table 3, Fig. 11D). In the first half of stance, the mechanical energy of the CoM decreased significantly from $E_{touchdown} = 1.00 \pm 0.00$ at touchdown to $E_{mid-stance} = 0.86 \pm 0.09$ at mid-stance (ANOVA, $F_{2,18} = 6.6132$, $P = 0.007$; Tukey's HSD). In the second half of stance, the mechanical energy of the CoM recovered to $E_{aerial} = 0.99 \pm 0.10$ at mid aerial phase, not significantly different from $E_{touchdown}$ (Tukey's HSD). The reduction in CoM mechanical energy in the first half of stance, $\Delta E_{mech} = 0.14 \pm 0.09$, is the mechanical work needed per step on the granular surface. By integration of F_z over vertical displacement of the foot during stance (see Appendix), the energy lost to the granular substrate ($E_{substrate}$) per step was estimated as 0.17 ± 0.05 , not significantly different from ΔE_{mech} (ANOVA, $F_{1,12} = 0.4659$, $P = 0.5078$). Note that the energies of each run were normalized to $E_{touchdown}$ of that run.

DISCUSSION

Conservation of spring-mass-like CoM dynamics on solid and granular surfaces

The observed kinematics and calculated mechanical energetics demonstrated that the zebra-tailed lizard ran like a spring-mass

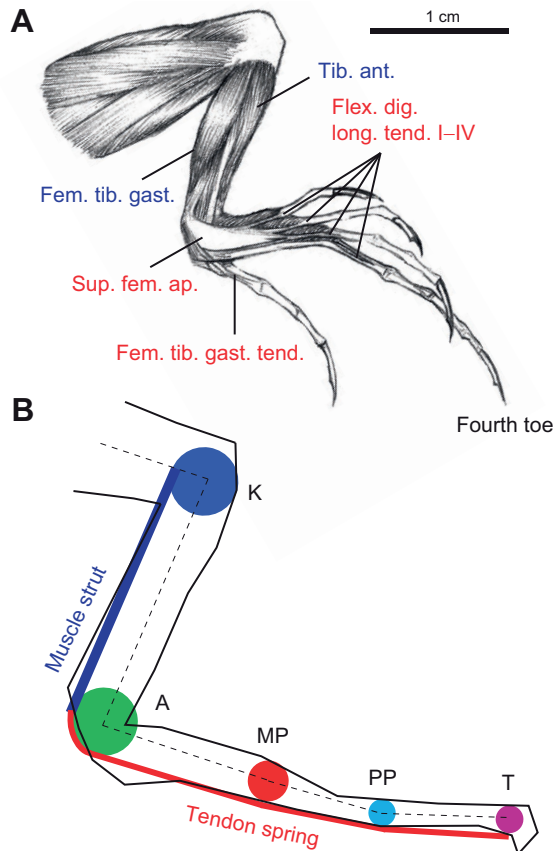


Fig. 7. Anatomy and a strut-spring model of the hind limb. (A) Ventral anatomy of a dissected hind limb. Lower hind leg muscles are marked in blue; foot tendons are marked in red. (B) A two-dimensional model of the hind limb. The muscle strut models isometrically contracting lower leg muscles; the tendon spring models foot tendons. The radii of colored circles correspond to measured joint radii.

system on both solid and granular surfaces. On both surfaces, the CoM forward speed (Fig. 5B), vertical position (Fig. 5C) and lateral position (Fig. 5D) displayed oscillation patterns that were in accord with predictions from the SLIP model (Blickhan, 1989) and the LLS model (Schmitt et al., 2002). The small relative oscillations of the CoM forward speed (i.e. $\Delta v_{x,CoM}/v_{x,CoM} \ll 1$) were expected because the Froude number was large for the lizard (see Appendix). The substantial sprawling of the legs contributed to the medio-lateral oscillatory motion of the animal. Furthermore, on both surfaces, the mechanical energy of the CoM oscillated within a step, reaching a minimum at mid-stance and a maximum during the aerial phase (Fig. 9F, Fig. 11D), a defining feature of spring-mass-like running (Blickhan, 1989; Schmitt et al., 2002).

To our knowledge, ours is the first study to quantitatively demonstrate spring-mass-like CoM motion in lizards running on granular surfaces. Spring-mass-like CoM motion was previously observed in other lizards and geckos running on solid surfaces (Farley and Ko, 1997; Chen et al., 2006), but it was not clear whether energy savings by elastic elements played an important role.

Hind foot function on the solid surface: energy-saving spring

Our study is the first to quantify elastic energy savings in foot tendons in lizards during running on solid surfaces. The significant energy savings (~40% of the mechanical work needed per step) in the zebra-tailed lizard's hind foot tendons is in a similar range to

the energy savings by ankle extensor tendons and digital flexor tendons and ligaments in larger animals (Alexander, 2003), such as kangaroos [50% (Alexander and Vernon, 1975)], wallabies [45% (Biewener et al., 1998)], horses [40% (Biewener, 1998b)] and humans [35%, with an additional 17% from ligaments in the foot arch (Ker et al., 1987)].

This is surprising considering that the elastic energy-saving mechanism was previously thought to be less important in small animals [e.g. 14% in hopping kangaroo rats of ~100 g mass (Biewener et al., 1981)]. Because the tendons of small animals are 'overbuilt' to withstand large stresses during escape, during steady-speed locomotion these tendons usually experience stresses too small to induce significant elastic energy storage and return (Biewener and Blickhan, 1988; McGowan et al., 2008). We verified that for zebra-tailed lizards running at $\sim 1 \text{ m s}^{-1}$, the maximal stress in the foot tendons is 4.3 MPa (see Appendix), well below the 100 MPa breaking stress for most tendons (Kirkendall and Garrett, 1997).

The zebra-tailed lizard's elongate hind foot and digitigrade foot posture on the solid surface may be an adaptation for elastic energy savings during rapid locomotion. Like other iguanids (Russell, 1993), this lizard does not have substantial ankle extensor tendons as large animals do. Nevertheless, elongation of foot tendons and a digitigrade posture enhance the hind foot's energy-saving capacity by decreasing tendon stiffness and mechanical advantage (Biewener et al., 2004) (see Appendix). A recent study also found significant energy savings (53%) by elongate foot tendons in running ostriches (Rubenson et al., 2011). More generally, elongation of distal limb segments such as legs, feet and toes, which possess tendons, may be an adaptation for energy saving during rapid locomotion. Indeed, many cursorial animals including mammals (Garland and Janis, 1993), lizards (Bauwens et al., 1995) and dinosaurs (Coombs, 1978) display elongation of distal limb segments. Short fascicles and long tendons and ligaments are often found in the ankle extensor muscles and digital flexor muscles in large cursorial ungulates such as horses, camels and antelopes (Alexander, 2003).

Solid surface model assumptions

Our estimates of elastic energy storage and return on the solid surface assume isometric contraction of lower leg muscles. However, muscles have a finite stiffness and do lengthen by a small amount under limb tension (Biewener, 1998a; Roberts et al., 1997). Despite this difference, our estimates still hold, because in the latter case both lower leg muscles and foot tendons behave like springs, and the total stiffness remains the same (because external force and total deformation remain the same). In the case where the muscles actively shorten during stance and further lengthen the tendons (which does positive mechanical work on the tendons), the energy storage and return in the tendons would increase. However, the overall energy efficiency would decrease (with everything else being the same), because apart from energy lost in tendon recoil, energy is further lost in the muscles that perform the mechanical work, i.e. muscle work is more expensive than tendon work (Biewener and Roberts, 2000).

In addition, the hind limb resilience obtained from anesthetized lizards was assumed to be a good estimate for hind limb resilience in running lizards. This is based on our observations that resilience was independent of torque, angular displacement and loading rate, as well as previous findings that the damping properties of animal limbs are largely intrinsic to their structure and material properties (Weiss et al., 1988; Fung, 1993; Dudek and Full, 2006). Future studies using techniques such as tendon buckles (Biewener et al., 1998), sonomicrometry (Biewener et al., 1998), ultrasonography

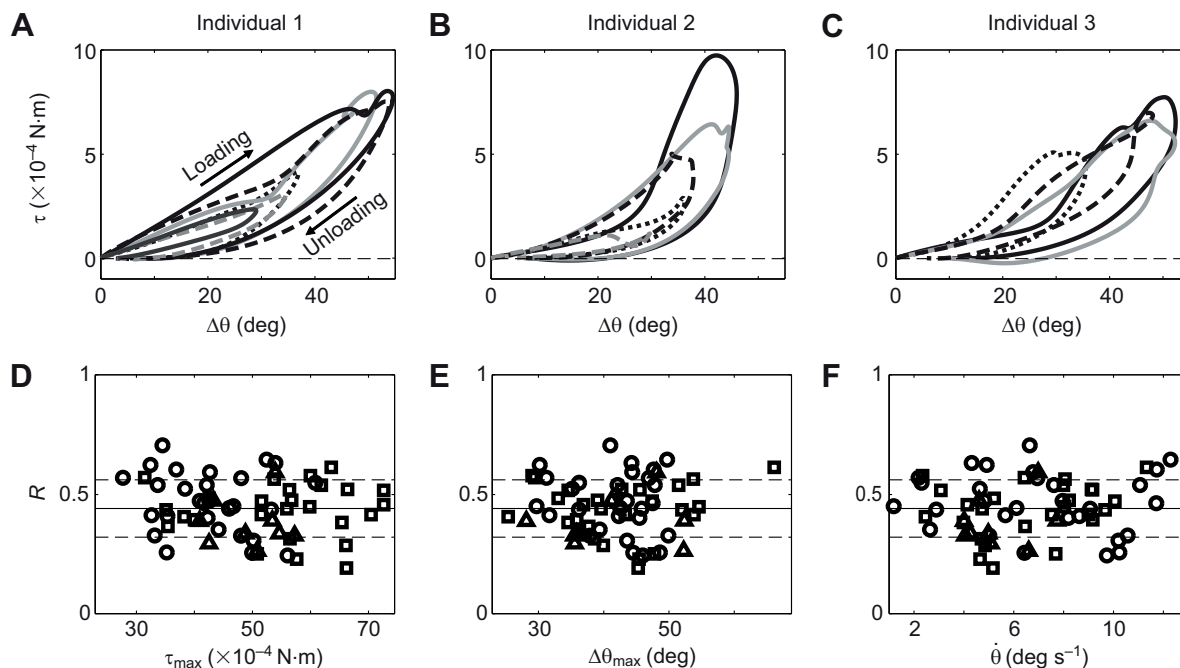


Fig. 8. Hind limb resilience. (A–C) Representative passive work loops of the hind foot (measured at the digit tip) from each of the three anesthetized lizards tested. Different curves are from different trials. The area within a work loop is the energy lost within the foot. See Fig. 2A for schematic of experimental setup. τ , torque; $\Delta\theta$, angular displacement. (D–F) Hind limb resilience (R) versus maximal torque (τ_{\max}), maximal angular displacement ($\Delta\theta_{\max}$) and loading rate ($\dot{\theta}$). Different symbols are from different individuals. Solid and dashed lines in D–F denote means \pm s.d., respectively.

(Maganaris and Paul, 1999) and oxygen consumption measurement (Alexander, 2003) during locomotion are needed to confirm this assumption.

Hind foot function on the granular surface: dissipative, force-generating paddle

The similarity between the observed and predicted $v_{z,\text{CoM}}$ on the granular surface supports the hypothesis of subsurface foot rotation. We speculate that on the granular surface the foot functions as a ‘paddle’ through fluidized particles to generate force. This differs from previous observations of the utilization of solidification forces of the granular media in a legged robot (Li et al., 2009; Li et al., 2010b) and sea turtle hatchlings (Mazouchova et al., 2010) moving on granular surfaces.

As the zebra-tailed lizard’s hind foot paddles through fluidized particles to generate force, energy is lost to the substrate because particle contact forces in granular media are dissipative (Nedderman, 1992). A large foot can reduce energy loss to the granular substrate compared with a small one, much like large snowshoes used by humans can reduce the energy cost of walking on snow (Knapik et al., 2002). From our model of foot–ground interaction on the granular surface, for a given animal (constant weight), energy loss to the substrate is proportional to foot penetration depth, and thus inversely proportional to foot area and substrate strength (see Appendix).

Granular surface model assumptions

In our modeling of the foot–ground interaction on the granular surface using the penetration force model, we made two assumptions. First, we assumed that the ground reaction forces were insensitive to speed. This is true in the low-speed regime [$<0.5 \text{ m s}^{-1}$ for our glass particles (Maladen et al., 2009)], where particle inertia is negligible and forces are dominated by particle friction. Because

friction is proportional to pressure, and pressure is proportional to depth (Hill et al., 2005), granular forces in the low-speed regime are proportional to depth ($F_z = \alpha|z|A$), analogous to the hydrostatic forces in fluids ($F_z = \rho g|z|A$, i.e. buoyant forces due to hydrostatic pressure).

Second, we used the vertical stress per unit depth α determined from vertical penetration of a horizontally oriented disc to estimate forces on the foot as it rotates subsurface. In this calculation, the effective vertical stress per unit depth $\alpha \cos\theta_{\text{foot}}$ (see Appendix) depended on foot orientation *via* a simple relationship, $\cos\theta_{\text{foot}}$ (because projected area $A = A_{\text{foot}} \cos\theta_{\text{foot}}$; see Appendix), and not on direction of motion. However, our recent physics experiments (Li et al., in preparation) suggest that stresses in granular media in the low-speed regime depend on both orientation and direction of motion in a more complicated manner, and that $\alpha \cos\theta_{\text{foot}}$ overestimates vertical stress per unit depth for all foot orientations and directions of motion except when the foot is horizontal and moving vertically downwards. Therefore, our model must be overestimating hydrostatic-like forces, and there must be additional forces contributing to the lizard’s ground reaction forces.

We propose that these additional forces are likely from hydrodynamic-like inertial forces resulting from the local acceleration of the substrate (particles) by the foot. Analogous to hydrodynamic forces in fluids (Vogel, 1996), for an intruder moving rapidly in granular media, the particles initially at rest in front of the intruder are accelerated by, and thus exert reaction forces on, the intruder. Hydrodynamic-like forces at $\sim 1 \text{ m s}^{-1}$ can play an important role both in impact forces on free-falling intruders (Katsuragi and Durian, 2007; Goldman and Umbanhowar, 2008) and in legged locomotion of small lightweight robots (Qian et al., 2012). We note that the foot rotation hypothesis should hold regardless, because hydrodynamic-like forces are also proportional to projected area (Katsuragi and Durian, 2007).

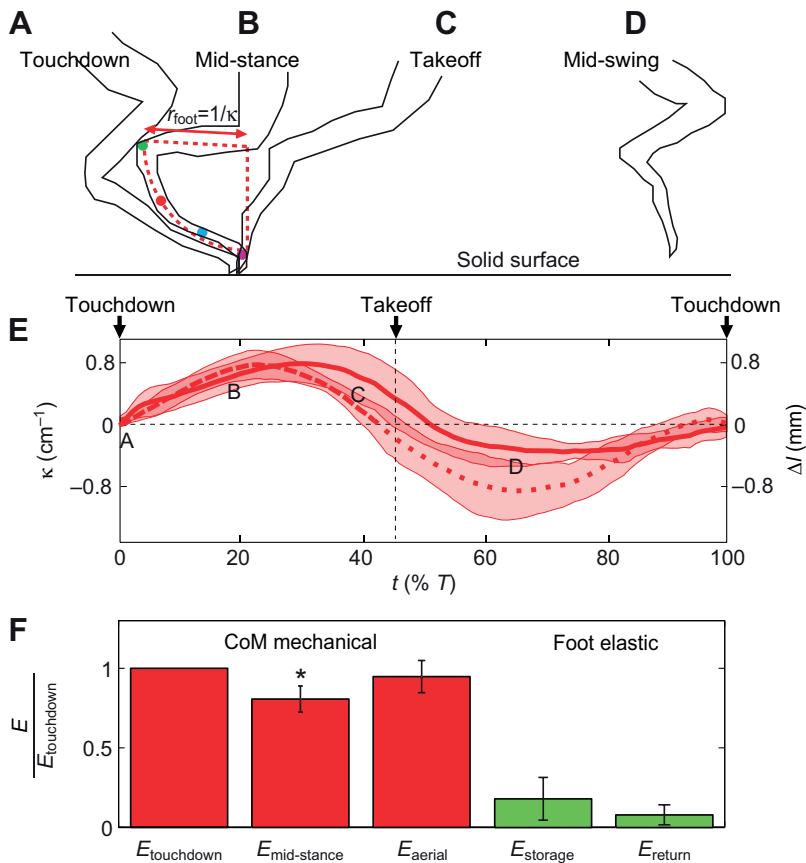


Fig. 9. Foot-ground interaction on the solid surface. (A–D) The hind foot shape from the lateral view of a representative run on the solid surface. A–D correspond to A–D in Fig. 3. The hind foot shape in the dorsal view is similar because the sprawl angle of the foot plane is nearly constant during stance. The diagram in B defines the radius of curvature (r_{foot}) of the foot (see Appendix). (E) Foot curvature (κ ; solid line) and tendon spring deformation (Δl ; dashed line) (means \pm s.d.) versus time during a stride on the solid surface. Tendon spring deformation is not meaningful during swing (dotted line) when the muscle strut assumption does not hold. (F) Mechanical energies of the CoM and elastic energies of the foot (means \pm s.d.) on the solid surface. See Table 3 for definitions and values of the energies. All energies (E) are normalized to the mechanical energy of the CoM at touchdown ($E_{\text{touchdown}}$) for each run. Asterisk indicates that $E_{\text{mid-stance}}$ is significantly different from $E_{\text{touchdown}}$ and E_{aerial} (ANOVA, Tukey's HSD, $P < 0.05$).

However, we know too little about the lizard's subsurface foot kinematics and the force laws in the high-speed regime on an intruder being pushed in a complex path within granular media (not simply a free-falling intruder) to more accurately calculate both hydrostatic-like and hydrodynamic-like forces. Future X-ray high-speed imaging experiments (Maladen et al 2009; Sharpe et al., in review) will reveal how the lizard foot was moving subsurface. Further studies of intrusion forces in granular media in both low-speed (Li et al., in preparation) and high-speed regimes can provide a more comprehensive understanding of ground reaction forces during legged locomotion on granular surfaces and provide better estimates of foot penetration depth and energy loss.

Comparison to water-running in the basilisk lizard

The rapid impact of the foot on the surface at touchdown and hypothesized subsurface foot rotation appear kinematically similar

to the slap and stroke phases of basilisk lizards running on the surface of water (Glasheen and McMahon, 1996a; Hsieh, 2003). For the zebra-tailed lizard running on sand, both granular hydrostatic-like and hydrodynamic-like forces can contribute to vertical ground reaction force. This is also qualitatively similar to water-running in the basilisk lizard, which utilizes both hydrostatic forces resulting from the hydrostatic pressure between the water surface and the bottom of the air cavity created by the foot, and hydrodynamic forces resulting from the water being accelerated from rest by the rapidly moving foot (Glasheen and McMahon, 1996a; Glasheen and McMahon, 1996b; Hsieh and Lauder, 2004).

However, the degree to which each species relies on these two categories of forces differs because of differences in the properties of the supporting media. For a given foot size, depth and speed, the hydrostatic forces in water are an order of magnitude smaller than

Table 3. Normalized energetic variables

Variable	Solid	Granular
Mechanical energy at touchdown, $E_{\text{touchdown}}$	1.00 \pm 0.00	1.00 \pm 0.00
Mechanical energy at mid-stance, $E_{\text{mid-stance}}$	0.81 \pm 0.08*	0.86 \pm 0.09*
Mechanical energy during aerial phase, E_{aerial}	0.95 \pm 0.10	0.99 \pm 0.10
Mechanical energy reduction, ΔE_{mech}	0.19 \pm 0.08	0.14 \pm 0.09
Elastic energy storage at mid-stance, E_{storage}	0.18 \pm 0.13	n/a
Elastic energy return, E_{return}	0.08 \pm 0.06	n/a
Energy loss to substrate, $E_{\text{substrate}}$	n/a	0.17 \pm 0.05
Muscle mechanical work, W_{muscle}	0.11 \pm 0.10	0.31 \pm 0.10

All energies were normalized to $E_{\text{touchdown}}$ for each run and averaged over seven representative runs on each surface.

Asterisks indicate a significant difference ($*P < 0.05$) in the mechanical energy of the CoM at mid-stance from that at touchdown and during the aerial phase. Data are means \pm s.d.

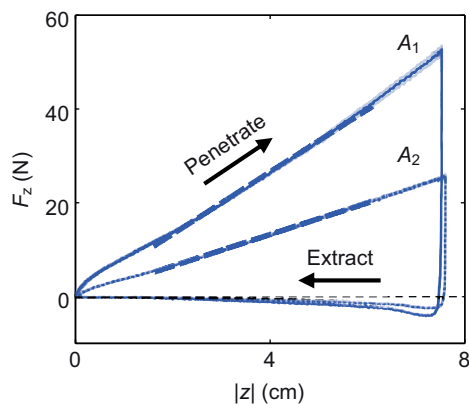


Fig. 10. Granular penetration force (means \pm s.d.) versus depth on two plates of different areas: $A_1=7.6\times 2.5\text{ cm}^2$ and $A_2=3.8\times 2.5\text{ cm}^2$. See Fig. 2B for schematic of experimental setup. Dashed blue lines are linear fits to the data over steady state during penetration using Eqn 1.

the hydrostatic-like forces in granular media, whereas the hydrodynamic(-like) forces are similar in water and in granular media (see Appendix). As a result, the basilisk lizard running on water must rely on hydrodynamic forces to a larger degree than the zebra-tailed lizard running on sand, considering that these two lizards are of similar size ($\sim 0.1\text{ m}$). An extreme example for this is that it is impossible for a basilisk lizard to stand on the surface of water, but a zebra-tailed lizard can stand on loose sand.

Motor function of upper hind leg

Despite the passive nature of the leg spring in the spring-mass model, animal limbs do not function purely passively as springs – the muscles within them must perform mechanical work. We have shown that on the solid surface, the lizard's hind foot saves $\sim 40\%$ of the mechanical work per step. The remaining 60% is lost either within the foot or to the ground, and must be compensated for by mechanical work performed by muscles, which is $W_{\text{muscle}}=0.11\pm 0.10$. This work is likely provided by knee extension during the second half of stance (Fig. 6D, red curve) powered by the upper leg muscles.

On the granular surface, substantial energy is lost to the substrate. This is in accord with previous observations of higher mechanical energetic cost during locomotion on granular surfaces in humans (Zamparo et al., 1992; Lejeune et al., 1998) and legged robots (Li et al., 2010a). Because the energy lost to the substrate equals the reduction in CoM mechanical energy during the first half of stance, even without energy loss within the limb, the upper hind leg muscles must perform mechanical work W_{muscle} of 0.31 ± 0.10 during the second half of stance, approximately three times that on the solid surface for a given animal running at a given speed, as evidenced by the larger knee extension on the granular surface (Fig. 6D, blue curve).

Our models of the foot-ground interaction on both surfaces assume purely passive foot mechanics, and do not consider the role of active neurosensory control. However, animals can actively adjust kinematics and muscle function to accommodate changes in surface conditions (Ferris et al., 1999; Daley and Biewener, 2006). We observed that when confronted by a substrate that transitioned from solid into granular (or *vice versa*), the lizard displayed partial adjustment of foot posture during the first step on the new surface, followed by full adjustment during the second step. Future studies using neuromechanics techniques, such as electromyography

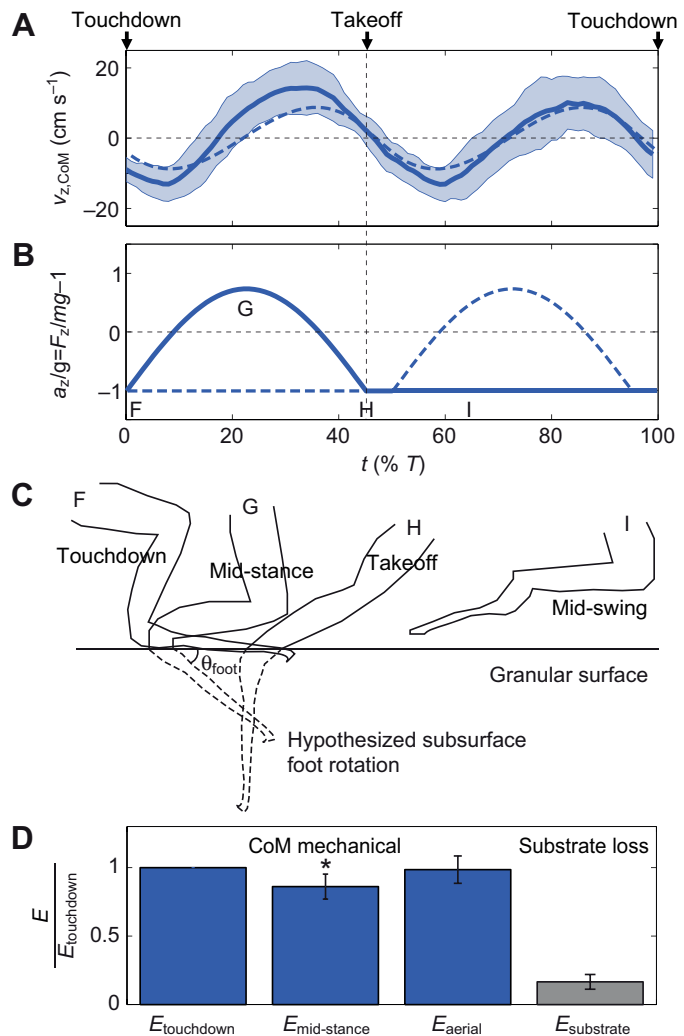


Fig. 11. Foot-ground interaction on the granular surface. (A) CoM vertical speed (means \pm s.d.) versus time during a stride. The solid curve is from the experiment. The dashed curve is calculated from the vertical acceleration from the model. (B) Vertical acceleration (normalized by g) versus time during a stride calculated from the total vertical ground reaction force F_z on both feet and the animal weight mg . Solid and dashed curves are the F_z on the two alternating hind feet. (C) Hypothesized subsurface foot rotation in the sagittal plane. F–I correspond to F–I in Fig. 3. θ_{foot} , foot angle in the sagittal plane. (D) Mechanical energy of the CoM and the energy loss to the substrate (means \pm s.d.) during running on the granular surface. See Table 3 for definitions and values of the energies. All energies (E) are normalized to the mechanical energy of the CoM at touchdown ($E_{\text{touchdown}}$) for each run. Asterisk indicates that $E_{\text{mid-stance}}$ is significantly different from $E_{\text{touchdown}}$ and E_{aerial} (ANOVA, Tukey's HSD, $P<0.05$).

(Biewener et al., 1998; Sponberg and Full, 2008; Sharpe et al., in review) and denervation and reinnervation (Chang et al., 2009), can determine how neural control and sensory feedback mechanisms are used to control limb function to accommodate changing substrates.

Conclusions

During running on both solid and granular surfaces, the zebra-tailed lizard displayed spring-mass-like CoM kinematics with distinct hind foot, hind leg and trunk kinematics. The lizard's large, elongate hind foot served multiple functions during locomotion.

On the solid surface, the hind foot functioned as an energy-saving spring and reduced ~40% of the mechanical work needed for each footstep. On the granular surface, the hind foot paddled through fluidized particles to generate force, and substantial energy was lost during irreversible deformation of the granular substrate. The energy lost within the foot and to the substrate must be compensated for by mechanical work done by the upper hind leg muscles.

The multifunctional hind foot may passively (and possibly actively) adjust to the substrate during locomotion in natural terrain, and provide this desert generalist with energetic advantages and simplify its neurosensory control tasks (Full and Koditschek, 1999). Current robotic devices often suffer low mobility and high cost of transport on flowing substrates such as granular material (Kumagai, 2004; Li et al., 2009; Li et al., 2010a; Li et al., 2010b; Matson, 2010). Insights from studies such as ours can provide inspiration for next-generation multi-terrain robots (Pfeifer et al., 2007). Finally, our study also highlights the need for comprehensive force models for granular media (Li et al., in preparation) and for flowing terrestrial environments in general.

APPENDIX

Small relative oscillation in forward speed

Running at 1.1 m s^{-1} , the lizard's Froude number in the sagittal plane was $Fr = v_{x, \text{CoM}}^2 / gL_0 = 3$ (where $L_0 \approx 4 \text{ cm}$ is the leg length at touchdown), above the typical value of 2.5 where most animals transition from trotting to galloping (Alexander, 2003). This implied that the kinetic energy ($\frac{1}{2}mv_{\text{CoM}}^2 \approx \frac{1}{2}mv_{x, \text{CoM}}^2$) of the CoM was three times larger than its gravitational potential energy (mgz_{CoM}). Because both the forward speed oscillation $\Delta v_{x, \text{CoM}}$ and vertical speed oscillation $\Delta v_{z, \text{CoM}}$ were determined by the total ground reaction force and the attack angle of the leg spring [$\beta = \sin^{-1}(v_{x, \text{CoM}}DT/2L_0) = 0.9 \text{ rad}$], they must be of the same order of magnitude (Blickhan, 1989), i.e. $\Delta v_{x, \text{CoM}} \sim \Delta v_{z, \text{CoM}}$. From the observed CoM kinematics, $\Delta v_{z, \text{CoM}} < (gL_0)^{1/2}$. Therefore, $\Delta v_{x, \text{CoM}} \sim \Delta v_{z, \text{CoM}} < (gL_0)^{1/2} \ll v_{x, \text{CoM}}$, and $\Delta v_{x, \text{CoM}}/v_{x, \text{CoM}} \ll 1$.

Hind foot curvature on the solid surface

Three-dimensional kinematics showed that the hind limb (from the hip to the digit tip of the fourth toe) remained nearly within a plane during the entire stride (out-of-plane component is 5% averaged over the entire stride). During stance, the orientation of the foot plane remained nearly unchanged, with a foot sprawl angle of $53 \pm 4 \text{ deg}$ relative to the sagittal plane in the posterior view. Hind foot curvature κ could then be obtained by fitting a circle to the hind foot (from the ankle to the digit tip) within the foot plane and determining the radius of curvature r_{foot} of the fit circle (see Fig. 9A), i.e. $\kappa = \pm 1/r_{\text{foot}}$, where a positive sign indicates foot hyperextension, a negative sign indicates foot flexion and a value of 0 indicates a straight foot.

Tendon spring deformation

From the two-dimensional strut-spring model of the hind limb, by geometry, the tendon spring deformation Δl was related to the observed changes of joint angles and the foot joint radii as: $\Delta l = \sum r_i \Delta \theta_i$, where $i = K, A, MP, PP$ (the four joints in the model), $\Delta \theta_i$ is the observed change in joint angle and r_i is the joint radius ($r_K = r_A = 1.25 \text{ mm}$, $r_{MP} = 0.75 \text{ mm}$, $r_{PP} = 0.50 \text{ mm}$). We observed that the relaxed hind foot of a live animal was nearly straight (Fig. 1A), which was similar to the foot shape at touchdown during running (Fig. 3A,E). Thus we defined the relaxed length of the tendon spring as the length when the foot was straight, i.e. $\Delta l = 0$ at touchdown.

The calculated maximal tendon spring deformation $\Delta l_{\text{max}} = 0.78 \text{ mm}$ corresponded to a 3% strain. We did not consider tendon spring deformation in the swing phase (dotted curve in Fig. 6F) because the assumption of isometric contraction of lower leg muscles was only valid for the stance phase.

Tendon spring stiffness

The stiffness of the tendon spring was defined as the maximal tension divided by the maximal deformation of the tendon spring, i.e. $k = T_{\text{max}}/\Delta l_{\text{max}}$. From the observed CoM kinematics, the total ground reaction force at mid-stance was $F_{\text{max}} = 0.3 \text{ N}$ within the coronal plane and pointed from the digit tip to the hip. At mid-stance, because the foot was neither dorsiflexing nor plantarflexing, torque was balanced at the ankle, i.e. $T_{\text{max}}r_A = F_{\text{max}}\Delta x_{AT}$, where $\Delta x_{AT} = 1.4 \text{ cm}$ was the horizontal distance between the ankle and the digit tip at mid-stance, and $r_A = 1.25 \text{ mm}$. Thus $T_{\text{max}} = 3.4 \text{ N}$ and $k = 4.4 \times 10^3 \text{ N m}^{-1}$. The maximal stress in the foot tendons during stance was $\sigma_{\text{max}} = T_{\text{max}}/\pi r_{\text{PP}}^2 = 4.3 \text{ MPa}$.

The torsional stiffness of the ankle observed in anesthetized lizards from the modified work loop experiments ($\sim 1 \times 10^{-3} \text{ Nm rad}^{-1}$) was an order of magnitude smaller than that estimated from running kinematics ($12 \times 10^{-3} \text{ Nm rad}^{-1}$). This is, however, not contradictory but expected because during stance the lizard's lower leg muscles must be activated, and the resulting higher tension from muscle contraction increases limb stiffness (Weiss et al., 1988).

Foot elongation increases energy savings on the solid surface

The stiffness of a piece of elastic material like a tendon is $k = E_0 A_0 / l_0$, where E_0 is the Young's modulus, A_0 is the cross-sectional area and l_0 is the rest length of the material. Most animal tendons are primarily made of collagen (Kirkendall and Garrett, 1997) and have similar Young's modulus values (i.e. E_0 is nearly constant). Thus, the stiffness of the tendon spring scales as $k \propto A_0 / l_0 \propto r_0^2 / l_0$, i.e. an elongate tendon (smaller radius r_0 and larger rest length l_0) is less stiff and stretches more easily than a short, thick tendon. Because elastic energy storage decreases with tendon stiffness ($E_{\text{storage}} = \frac{1}{2}k\Delta l_{\text{max}}^2 = \frac{1}{2}T_{\text{max}}^2/k \propto 1/k$ for a given T_{max}), an elongate tendon can store (and return) more energy.

An elongate foot also reduces the moment arm of tendon tension (small r_A) but increases the moment arm of the ground reaction force (large Δx_{AT}) about the ankle, therefore reducing the mechanical advantage (Biewener et al., 2004), so it increases tension in the foot for a given ground reaction force (because $T_{\text{max}} = F_{\text{max}}\Delta x_{AT}/r_A$) and amplifies tendon stretch for enhanced energy storage and return.

Vertical ground reaction force on the granular surface

We assumed that the hind foot was rotating at a constant angular velocity in the sagittal plane ω about the moving ankle during stance, i.e. the foot angle in the sagittal plane $\theta_{\text{foot}} = \omega t$ within $0 \leq t \leq DT$ and $0 \leq \theta_{\text{foot}} \leq \pi/2$, then $\omega = \pi/2DT = 10\pi/9T = 35 \text{ rad s}^{-1}$. From the measured vertical speed of the ankle and this assumed foot rotation, the vertical speed of most (75%) of the foot was always below 0.5 m s^{-1} during most (75%) of stance.

Given foot rotation $\theta_{\text{foot}} = \omega t$, the foot area projected in the horizontal plane decreased with time as $A = A_{\text{foot}} \cos \omega t$, where $A_{\text{foot}} = 1 \text{ cm}^2$ is the hind foot area; the foot depth (measured at the center of the foot) increased with time as $|z| = |z|_{\text{max}} \sin \omega t$, where $|z|_{\text{max}}$ is the maximal foot depth during stance. The vertical ground reaction force on the foot was then sinusoidal: $F_z = F_{z, \text{max}} \sin 2\omega t$, where $F_{z, \text{max}} = \alpha A_{\text{foot}} |z|_{\text{max}} \sin \pi/4 \cos \pi/4 = \frac{1}{2} \alpha A_{\text{foot}} |z|_{\text{max}}$ is the maximal vertical ground reaction force on a hind foot. For steady-state locomotion on

a level surface, the F_z generated by one foot averaged over a cycle must equal half the body weight, i.e.:

$$\int_0^T F_{z,\max} \sin 2\omega t \, dt = \frac{1}{2} mg. \quad (\text{A1})$$

Therefore, $F_{z,\max} = 5\pi mg/9$ and $F_z = 5\pi mg/9 \sin 10\pi t/9T$.

Energy loss to the granular surface

By integration of vertical ground reaction force over vertical displacement of the foot, the energy loss to the granular surface was:

$$E_{\text{substrate}} = \int_0^{|z|_{\max}} F_z dz = \int_0^T F_z \frac{d|z|}{dt} dt, \quad (\text{A2})$$

where $|z|_{\max} = 1.0$ cm from $F_{z,\max} = \frac{1}{2} \alpha A_{\text{foot}} |z|_{\max}$. The hypothesized foot rotation in the sagittal plane did not take into account the sprawl of the foot during stance, which could induce additional energy loss by lateral displacement of the granular surface. However, a sprawled foot posture did not affect the condition of vertical force balance and thus did not change our estimate of energy dissipation in the sagittal plane. Therefore this estimate provides a lower bound.

Large foot area reduces energy loss on the granular surface

For a given animal (constant weight mg), $F_{z,\max} = \frac{1}{2} \alpha A_{\text{foot}} |z|_{\max} = 5\pi mg/9$ is constant, thus:

$$E_{\text{substrate}} = |z|_{\max} \int_0^T F_z \omega \cos \omega t \, dt \propto |z|_{\max} \propto 1/(\alpha A_{\text{foot}}). \quad (\text{A3})$$

This implies that the energy loss to the granular surface increases with foot penetration depth. On a given granular surface (fixed α), a larger foot (larger A_{foot}) sinks less than a smaller foot, and thus loses less energy to the substrate. For a given foot size (fixed A_{foot}), a foot sinks less on a stronger granular surface (larger α) than on a weaker surface, and thus loses less energy to the substrate.

Comparison of forces in granular media and in water

For water, hydrostatic force is $F_z = \rho g |z| A$. Comparing this with $F_z = \alpha |z| A$ for granular media, ρg is the equivalent of α . For water, $\rho g = 1.0 \times 10^4 \text{ N m}^{-3}$; for loosely packed glass particles, $\alpha = 3.5 \times 10^5 \text{ N m}^{-3}$. Therefore, the hydrostatic forces in water are an order of magnitude smaller than the hydrostatic-like forces in granular media for given foot size and depth.

Hydrodynamic(-like) forces should be proportional to the density of the surrounding media because they are due to the media being accelerated. For water, $\rho = 1.0 \times 10^3 \text{ N m}^{-3}$; for loosely packed glass particles the effective density is $(2.5 \times 10^3 \text{ N m}^{-3}) \times (0.58 \text{ volume fraction}) = 1.45 \times 10^3 \text{ N m}^{-3}$. Therefore, the hydrodynamic forces in water and hydrodynamic-like forces in granular media are on the same order of magnitude for given foot size and foot speed.

LIST OF SYMBOLS AND ABBREVIATIONS

A	ankle
A	area (projected into the horizontal plane)
A_0	cross-sectional area of a piece of elastic material
A_1, A_2	area of the two plates used in the penetration force measurements
A_{foot}	foot area
a_z	net vertical acceleration due to F_z on one hind foot and animal weight
CoM	center of mass
D	duty factor
E_0	Young's modulus of a piece of elastic material

E_{aerial}	CoM mechanical energy at mid aerial phase
$E_{\text{mid-stance}}$	CoM mechanical energy at mid-stance
E_{return}	elastic energy returned in the second half of stance
E_{storage}	elastic energy stored in the tendon spring at mid-stance
$E_{\text{substrate}}$	energy lost to the granular substrate
$E_{\text{touchdown}}$	CoM mechanical energy at touchdown
f	stride frequency
F	ground reaction force
F_{max}	ground reaction force at mid-stance
Fr	Froude number
F_z	vertical ground reaction force
$F_{z,\max}$	maximal vertical ground reaction force on a hind foot
g	gravitational acceleration
H	hip
HSD	honestly significant difference
k	tendon spring stiffness
K	knee
l_0	rest length of a piece of elastic material
L_0	leg length at touchdown
LLS	lateral leg spring
m	animal mass
mg	animal weight
MP	metatarsal-phalangeal joint of the fourth toe
N	neck
P	pelvis
PP	distal end of the proximal phalanx of the fourth toe
R	hind limb resilience
r_0	radius of a piece of elastic material
r_{foot}	radius of curvature of the hind foot
r_i	radius of joint i
SLIP	spring-loaded inverted pendulum
SVL	snout-vent length
t	time
T	digit tip of the fourth toe
T	stride period
T_{max}	maximal tension in the foot tendons
v_{CoM}	CoM total speed
$v_{x,\text{CoM}}$	forward speed
$\bar{v}_{x,\text{CoM}}$	mean forward speed
$v_{z,\text{CoM}}$	CoM vertical speed
W_{muscle}	muscle mechanical work
y_{CoM}	CoM lateral position
z_{CoM}	CoM height
\bar{z}_{CoM}	mean CoM height
z_{knee}	knee height
z_{pelvis}	pelvis height
\bar{z}_{pelvis}	mean pelvis height
$ z $	depth
$ z _{\max}$	maximal foot depth during stance
α	vertical stress per unit depth
β	attack angle of the leg spring
ΔE_{mech}	reduction in CoM mechanical energy during the first half of stance, or mechanical work needed per step
Δl	tendon spring deformation
Δl_{max}	maximal tendon spring deformation
$\Delta v_{x,\text{CoM}}$	magnitude of CoM forward speed oscillations
Δx_{AT}	horizontal distance between the ankle and the digit tip at mid-stance
Δy_{CoM}	magnitude of CoM lateral oscillations
Δz_{CoM}	magnitude of CoM vertical oscillations
Δz_{knee}	knee vertical displacement during the first half of stance
$\Delta \theta$	angular displacement of the foot
$\Delta \theta_i$	change in the joint angle of joint i
$\Delta \theta_{\text{knee}}$	knee joint extension during the first half of stance
$\Delta \theta_{\text{max}}$	maximal angular displacement of the foot
κ	foot curvature
λ	stride length
$\dot{\theta}$	loading rate
θ_0	angle between the ankle and the digit tip in the relaxed, straight foot
θ_{foot}	foot angle in the sagittal plane

θ_{knee}	knee angle
θ_{pitch}	trunk pitch angle
$\bar{\theta}_{\text{pitch}}$	mean trunk pitch angle
θ_{sprawl}	leg sprawl angle
$\bar{\theta}_{\text{sprawl}}$	mean leg sprawl angle during stance
θ_t	angle between the ankle and the digit tip in the hyperextended foot
$\theta_{\text{touchdown}}$	touchdown foot angle
ρ	density
σ_{max}	maximal stress in the foot tendons
τ	torque about the ankle joint
τ_{max}	maximal torque
ω	angular velocity of the foot in the sagittal plane

ACKNOWLEDGEMENTS

We gratefully thank Sarah Sharpe, Yang Ding, Nick Gravish, Ryan Maladen, Paul Umbanhowar, Wyatt Korff, Kyle Mara, Young-Hui Chang, Andy Biewener, Tom Roberts, Craig McGowan, Bob Full and two anonymous reviewers for helpful discussions and/or comments on the manuscript; Loretta Lau for help with kinematics data digitization; Sarah Sharpe for help with animal protocol and anesthesia; Mateo Garcia, Nick Gravish and Andrei Savu for help with force plate setup; Ryan Maladen and The Sweeney Granite Mountains Desert Research Center for help with animal collection; and the staff of The Physiological Research Laboratory animal facility of The Georgia Institute of Technology for animal housing and care.

FUNDING

This work was funded by The Burroughs Wellcome Fund (D.I.G. and C.L.), The Army Research Laboratory (ARL) Micro Autonomous Systems and Technology (MAST) Collaborative Technology Alliance (CTA) under cooperative agreement number W911NF-08-2-0004 (D.I.G. and C.L.), The Army Research Office (D.I.G. and C.L.), National Science Foundation Foundation Physics of Living Systems (D.I.G.) and Temple University start-up funds (S.T.H.).

REFERENCES

- Alexander, R. M. (2003). *Principles of Animal Locomotion*. Princeton, NJ: Princeton University Press.
- Alexander, R. M. and Vernon, A. (1975). The mechanics of hopping by kangaroos (Macropodidae). *J. Zool.* **177**, 265-303.
- Autumn, K., Liang, Y. A., Hsieh, S. T., Zesch, W., Chan, W. P., Kenny, T. W., Fearing, R. S. and Full, R. J. (2000). Adhesive force of a single gecko foot-hair. *Nature* **405**, 681-685.
- Bauwens, D., Garland, T., Jr, Castilla, A. M. and Van Damme, R. (1995). Evolution of sprint speed in lacertid lizards: morphological, physiological and behavioral covariation. *Evolution* **49**, 848-863.
- Biewener, A. A. (1998a). Muscle function *in vivo*: a comparison of muscles used for elastic energy savings versus muscles used to generate mechanical power. *Integr. Comp. Biol.* **38**, 703-717.
- Biewener, A. A. (1998b). Muscle-tendon stresses and elastic energy storage during locomotion in the horse. *Comp. Biochem. Physiol.* **120B**, 73-87.
- Biewener, A. A. and Blickhan, R. (1988). Kangaroo rat locomotion: design for elastic energy storage or acceleration? *J. Exp. Biol.* **140**, 243-255.
- Biewener, A. A. and Roberts, T. J. (2000). Muscle and tendon contributions to force, work, and elastic energy savings: a comparative perspective. *Exerc. Sport Sci. Rev.* **28**, 99-107.
- Biewener, A. A., Alexander, R. M. and Heglund, N. C. (1981). Elastic energy storage in the hopping of kangaroo rats (*Dipodomys spectabilis*). *J. Zool.* **195**, 369-383.
- Biewener, A. A., Konieczynski, D. D. and Baudinette, R. V. (1998). *In vivo* muscle force-length behavior during steady-speed hopping in tammar wallabies. *J. Exp. Biol.* **201**, 1681-1694.
- Biewener, A. A., Farley, C. T., Roberts, T. J. and Temaner, M. (2004). Muscle mechanical advantage of human walking and running: implications for energy cost. *J. Appl. Physiol.* **97**, 2266-2274.
- Blickhan, R. (1989). The spring-mass model for running and hopping. *J. Biomech.* **22**, 1217-1227.
- Blickhan, R. and Full, R. J. (1993). Similarity in multilegged locomotion: bouncing like a monopode. *J. Comp. Physiol.* **173**, 509-517.
- Chang, Y.-H., Auyang, A. G., Scholz, J. P. and Nichols, T. R. (2009). Whole limb kinematics are preferentially conserved over individual joint kinematics after peripheral nerve injury. *J. Exp. Biol.* **212**, 3511-3521.
- Chen, J. J., Peattie, A. M., Autumn, K. and Full, R. J. (2006). Differential leg function in a sprawled-posture quadrupedal trotter. *J. Exp. Biol.* **209**, 249-259.
- Coombs, W. P., Jr (1978). Theoretical aspects of cursorial adaptations in dinosaurs. *Q. Rev. Biol.* **53**, 393-418.
- Crawford, C. S. (1981). *Biology of Desert Invertebrates*. New York: Springer.
- Daley, M. A. and Biewener, A. A. (2006). Running over rough terrain reveals limb control for intrinsic stability. *Proc. Natl. Acad. Sci. USA* **103**, 15681-15686.
- Dickinson, M. H., Farley, C. T., Full, R. J., Koehli, M. A. R., Kram, R. and Lehman, S. (2000). How animals move: an integrative view. *Science* **288**, 100-106.
- Dickinson, W. W. and Ward, J. D. (1994). Low depositional porosity in eolian sands and sandstones, Namib Desert. *J. Sediment. Res.* **64**, 226-232.
- Ding, Y., Gravish, N. and Goldman, D. I. (2011). Drag induced lift in granular media. *Phys. Rev. Lett.* **106**, 028001.
- Dudek, D. M. and Full, R. J. (2006). Passive mechanical properties of legs from running insects. *J. Exp. Biol.* **209**, 1502-1515.
- Farley, C. T. and Ko, T. C. (1997). Mechanics of locomotion in lizards. *J. Exp. Biol.* **200**, 2177-2188.
- Ferris, D. P., Louie, M. and Farley, C. T. (1998). Running in the real world: adjusting leg stiffness for different surfaces. *Proc. Biol. Sci.* **265**, 989-994.
- Ferris, D. P., Liang, K. and Farley, C. T. (1999). Runners adjust leg stiffness for their first step on a new running surface. *J. Biomech.* **32**, 787-794.
- Full, R. J. and Koditschek, D. E. (1999). Templates and anchors: neuromechanical hypotheses of legged locomotion on land. *J. Exp. Biol.* **202**, 3325-3332.
- Fung, Y. C. (1993). *Biomechanics: Mechanical Properties of Living Tissues*. New York: Springer.
- Garland, T., Jr and Janis, C. (1993). Does metatarsal/femur ratio predict maximal running speed in cursorial mammals? *J. Zool.* **229**, 133-151.
- Glasheen, J. W. and McMahon, T. A. (1996a). A hydrodynamic model of locomotion in the basilisk lizard. *Nature* **380**, 340-342.
- Glasheen, J. W. and McMahon, T. A. (1996b). Vertical water entry of disks at low Froude numbers. *Phys. Fluids* **8**, 2078-2083.
- Goldman, D. I. and Umbanhowar, P. B. (2008). Scaling and dynamics of sphere and disk impact into granular media. *Phys. Rev. E* **77**, 021308.
- Gravish, N., Umbanhowar, P. B. and Goldman, D. I. (2010). Force and flow transition in plowed granular media. *Phys. Rev. Lett.* **105**, 208301.
- Hedrick, T. L. (2008). Software techniques for two- and three-dimensional kinematic measurements of biological and biomimetic systems. *Bioinspir. Biomim.* **3**, 034001.
- Hill, G., Yeung, S. and Koehler, S. A. (2005). Scaling vertical drag forces in granular media. *Eur. Phys. J. Lett.* **72**, 137-143.
- Holmes, P., Full, R. J., Koditschek, D. and Guckenheimer, J. (2006). The dynamics of legged locomotion: models, analyses, and challenges. *SIAM Rev.* **48**, 207-304.
- Hsieh, S. T. (2003). Three-dimensional hindlimb kinematics of water running in the plumed basilisk lizard (*Basiliscus plumifrons*). *J. Exp. Biol.* **206**, 4363-4377.
- Hsieh, S. T. and Lauder, G. V. (2004). Running on water: three-dimensional force generation by basilisk lizards. *Proc. Natl. Acad. Sci. USA* **101**, 16784-16788.
- Irschick, D. J. and Jayne, B. C. (1999a). Comparative three-dimensional kinematics of the hindlimb for high-speed bipedal and quadrupedal locomotion of lizards. *J. Exp. Biol.* **202**, 1047-1065.
- Irschick, D. J. and Jayne, B. C. (1999b). A field study of the effects of incline on the escape locomotion of a bipedal lizard, *Callisaurus draconoides*. *Physiol. Biochem. Zool.* **72**, 44-56.
- Jindrich, D. L. and Full, R. J. (1999). Many-legged maneuverability: dynamics of turning in hexapods. *J. Exp. Biol.* **202**, 1603-1623.
- Karasov, W. H. and Anderson, R. A. (1998). Correlates of average daily metabolism of field-active zebra-tailed lizards (*Callisaurus draconoides*). *Physiol. Zool.* **71**, 93-105.
- Katsuragi, H. and Durian, D. J. (2007). Unified force law for granular impact cratering. *Nat. Phys.* **3**, 420-423.
- Ker, R. F., Bennett, M. B., Bibby, S. R., Kester, R. C. and Alexander, R. M. (1987). The spring in the arch of the human foot. *Nature* **325**, 147-149.
- Kirkendall, D. T. and Garrett, W. E. (1997). Function and biomechanics of tendons. *Scand. J. Med. Sci. Sports* **7**, 62-66.
- Knapik, J. J., Hickey, C., Ortega, S., Nagel, J. and De Pontbriand, R. (2002). Energy cost during locomotion across snow: a comparison of four types of snowshoes with showshoe design considerations. *Work* **18**, 171-177.
- Korff, W. L. and McHenry, M. J. (2011). Environmental differences in substrate mechanics do not affect sprinting performance in sand lizards (*Uma scoparia* and *Callisaurus draconoides*). *J. Exp. Biol.* **214**, 122-130.
- Kumagai, J. (2004). Sand trap – DARPA's 320-kilometer robotic race across the Mojave Desert yields no winner, but plenty of new ideas. *IEEE Spectr.* **41**, 44-50.
- Lejeune, T. M., Willems, P. A. and Heglund, N. C. (1998). Mechanics and energetics of human locomotion on sand. *J. Exp. Biol.* **201**, 2071-2080.
- Li, C., Umbanhowar, P. B., Komsuoglu, H., Koditschek, D. E. and Goldman, D. I. (2009). Sensitive dependence of the motion of a legged robot on granular media. *Proc. Natl. Acad. Sci. USA* **106**, 3029-3034.
- Li, C., Hoover, A. M., Birkmeyer, P., Umbanhowar, P. B., Fearing, R. S. and Goldman, D. I. (2010a). Systematic study of the performance of small robots on controlled laboratory substrates. *Proc. SPIE Int. Soc. Opt. Eng.* **7679**, 1-13.
- Li, C., Umbanhowar, P. B., Komsuoglu, H. and Goldman, D. I. (2010b). The effect of limb kinematics on the speed of a legged robot on granular media. *Exp. Mech.* **50**, 1383-1393.
- Li, C., Zhang, T. and Goldman, D. I. (in preparation). Towards a terradynamics for locomotion on flowing ground.
- Maganaris, C. N. and Paul, J. P. (1999). *In vivo* human tendon mechanical properties. *J. Physiol.* **521**, 307-313.
- Maladen, R. D., Ding, Y., Li, C. and Goldman, D. I. (2009). Undulatory swimming in sand: subsurface locomotion of the sandfish lizard. *Science* **325**, 314-318.
- Maladen, R. D., Ding, Y., Umbanhowar, P. B., Kamor, A. and Goldman, D. I. (2011). Mechanical models of sandfish locomotion reveal principles of high performance subsurface sand-swimming. *J. R. Soc. Interface* **8**, 1332-1345.
- Matson, J. (2010). Unfree spirit: NASA's Mars rover appears stuck for good. *Sci. Am.* **302**, 16.
- Mazouchova, N., Gravish, N., Savu, A. and Goldman, D. I. (2010). Utilization of granular solidification during terrestrial locomotion of hatching sea turtles. *Biol. Lett.* **6**, 398-401.
- McGowan, C. P., Skinner, J. and Biewener, A. A. (2008). Hind limb scaling of kangaroos and wallabies (superfamily Macropodoidea): implications for hopping performance, safety factor and elastic savings. *J. Anat.* **212**, 153-163.
- Moritz, C. T. and Farley, C. T. (2003). Human hopping on damped surfaces: strategies for adjusting leg mechanics. *Proc. Biol. Sci.* **270**, 1741-1746.

- Mosauer, W.** (1932). Adaptive convergence in the sand reptiles of the Sahara and of California: a study in structure and behavior. *Copeia* **1932**, 72-78.
- Nedderman, R. M.** (1992). *Statics and Kinematics of Granular Materials*. Cambridge: Cambridge University Press.
- Pfeifer, R., Lungarella, M. and Iida, F.** (2007). Self-organization, embodiment, and biologically inspired robotics. *Science* **318**, 1088-1093.
- Qian, F., Zhang, T., Li, C., Masarati, P., Hoover, A. M., Birkmeyer, P., Pullin, A., Fearing, R. S. and Goldman, D. I.** (2012). Walking and running on yielding and fluidizing ground. *Proceedings of Robotics: Science and Systems* (in press).
- Roberts, T. J., Marsh, R. L., Weyand, P. G. and Taylor, C. R.** (1997). Muscular force in running turkeys: the economy of minimizing work. *Science* **275**, 1113-1115.
- Rubenson, J., Lloyd, D. G., Heliams, D. B., Besier, T. F. and Fournier, P. A.** (2011). Adaptations for economical bipedal running: the effect of limb structure on three-dimensional joint mechanics. *J. R. Soc. Interface* **8**, 740-755.
- Russell, A. P.** (1993). The aponeuroses of the lacertilian ankle. *J. Morphol.* **218**, 65-84.
- Schmitt, J., Garcia, M., Razo, R. C., Holmes, P. and Full, R. J.** (2002). Dynamics and stability of legged locomotion in the horizontal plane: a test case using insects. *Biol. Cybern.* **86**, 343-353.
- Sharpe, S. S., Ding, Y. and Goldman, D. I.** (in review). Environmental interaction influences muscle activation strategy during sand-swimming in the sandfish lizard (*Scincus scincus*). *J. Exp. Biol.*
- Spagna, J. C., Goldman, D. I., Lin, P.-C., Koditschek, D. E. and Full, R. J.** (2007). Distributed mechanical feedback in arthropods and robots simplifies control of rapid running on challenging terrain. *Bioinspir. Biomim.* **2**, 9-18.
- Spence, A. J., Revzen, S., Seipel, J., Mullens, C. and Full, R. J.** (2010). Insects running on elastic surfaces. *J. Exp. Biol.* **213**, 1907-1920.
- Sponberg, S. and Full, R. J.** (2008). Neuromechanical response of musculo-skeletal structures in cockroaches during rapid running on rough terrain. *J. Exp. Biol.* **211**, 433-446.
- Vitt, L. J. and Ohmart, R. D.** (1977). Ecology and reproduction of lower Colorado River lizards: I. *Callisaurus draconoides* (Iguanidae). *Herpetologica* **33**, 214-222.
- Vogel, S.** (1996). *Life in Moving Fluids: The Physical Biology of Flow*. Princeton, NJ: Princeton University Press.
- Weiss, P. L., Hunter, I. W. and Kearney, R. E.** (1988). Human ankle joint stiffness over the full range of muscle activation levels. *J. Biomech.* **21**, 539-544.
- Zamparo, P., Perini, R., Orizio, C., Sacher, M. and Ferretti, G.** (1992). The energy cost of walking or running on sand. *Eur. J. Appl. Physiol. Occup. Physiol.* **65**, 183-187.